

~~CONFIDENTIAL~~

Copy
RM L53T06

NACA RM L53T06



NACA

RESEARCH MEMORANDUM

WIND-TUNNEL TESTS OF A MODEL OF A WINGLESS FIN-CONTROLLED
MISSILE TO OBTAIN STATIC STABILITY AND CONTROL

CHARACTERISTICS THROUGH A RANGE OF

MACH NUMBERS FROM 0.5 TO 0.88

By Dale L. Burrows and Ernest E. Newman

Langley Aeronautical Laboratory
Langley Field, Va.

CLASSIFIED DOCUMENT

This material contains information affecting the National Defense of the United States within the meaning of the espionage laws, Title 18, U.S.C., Secs. 793 and 794, the transmission or revelation of which in any manner to an unauthorized person is prohibited by law.

**NATIONAL ADVISORY COMMITTEE
FOR AERONAUTICS**

WASHINGTON

April 12, 1954

~~CONFIDENTIAL~~

Classification cancelled (no need to declassified)

Approved by NASA Tech. Rep. Agreement #7...
6 - FOR AUTHORIZED TO CHANGE)

By 30 June 69
USC AND

..... NK
GRADE OF OFFICER MAKING CHANGE)

12 Dec 61
DATE



0144312

NACA RM L53J06

NATIONAL ADVISORY COMMITTEE FOR AERONAUTICS

RESEARCH MEMORANDUM

WIND-TUNNEL TESTS OF A MODEL OF A WINGLESS FIN-CONTROLLED
MISSILE TO OBTAIN STATIC STABILITY AND CONTROL
CHARACTERISTICS THROUGH A RANGE OF

MACH NUMBERS FROM 0.5 TO 0.88

By Dale L. Burrows and Ernest E. Newman

SUMMARY

An investigation at medium to high subsonic speeds has been conducted in the Langley low-turbulence pressure tunnel to determine the static stability and control characteristics and to measure the fin normal forces and moments for a model of a wingless fin-controlled missile. The data were obtained at a Reynolds number of 2.1×10^6 based on the missile maximum diameter or 17.7×10^6 based on missile length; this Reynolds number was found to be large enough to avoid any large scale effects between the test and the expected flight Reynolds number.

With the horizontal-fin deflection limited to a maximum of 6° , longitudinally stable and trimmed flight could not be maintained beyond an angle of attack of 17° for a Mach number of 0.88 and beyond 20° for a Mach number of 0.50 for any center-of-gravity location without the use of some auxiliary stability or control device such as jet vanes. Mach number had no appreciable effect on the center-of-pressure positions and only a slight effect on neutral-point position. There was a shift in neutral-point position of about 1 caliber as the angle of attack was varied through the range for which the neutral point could be determined. Yawing the model to angles of sideslip up to 7° had little effect on the longitudinal stability at angles of attack up to 15° ; however, above 15° , the effect of sideslip was destabilizing.

With the vertical fins at a $\pm 6^\circ$ roll deflection, the rolling moment caused by yawing the model at high angles of attack could be trimmed out up to angles of sideslip of 6.5° and an angle of attack of 26° for a Mach number of 0.50; this range of sideslip angles was reduced to 3° at a Mach number of 0.88. The data indicated that, at lower angles of attack, the trim range extended to higher angles of sideslip.

The total normal-force and hinge-moment coefficients for both horizontal fins were slightly nonlinear with both angle-of-attack and fin deflection. The effect of Mach number was to reduce the slopes of the hinge-moment coefficient with angle of attack and deflection angle. In general, the effect of increasing the sideslip angle was to reduce the values of the fin normal-force and hinge-moment coefficients.

CONFIDENTIAL

INTRODUCTION

In the launching of missiles from the earth's surface, the problem of stability and control may be especially critical in the subsonic speed range where high surface winds can impose serious conditions of high angles of attack and sideslip. Because there is a lack of data for controllable-fin missiles at subsonic speeds and at high angles of attack, a test program was conducted on a wingless fin-controlled missile model. The small 60° delta fins are mounted in cruciform at the missile base and may be deflected for missile control.

This report contains the results of tests conducted in the Langley low-turbulence pressure tunnel to determine the aerodynamic characteristics for the complete missile, fin control effectiveness, and fin forces and moments at Mach numbers from 0.5 to 0.88 for angles of attack to as high as 26° and for combinations of angle of attack and sideslip.

SYMBOLS

The coordinate system used and the directions of positive forces, moments, and angles are shown in figure 1.

C_N	normal-force coefficient, $\frac{\text{Normal force}}{qA}$
C_X	longitudinal-force coefficient, $\frac{\text{Longitudinal force}}{qA}$
C_Y	lateral-force coefficient, $\frac{\text{Lateral force}}{qA}$
C_l	rolling-moment coefficient, $\frac{\text{Rolling moment}}{qAd}$
C_m	pitching-moment coefficient, $\frac{\text{Pitching moment}}{qAd}$
C_L	lift coefficient, $\sin \alpha C_X + \cos \alpha C_N$
C_D	drag coefficient, $-\cos \alpha \cos \beta C_X - \sin \beta C_Y + \cos \beta \sin \alpha C_N$
C_n	yawing-moment coefficient, $\frac{\text{Yawing moment}}{qAd}$
C_{N_F}	fin normal-force coefficient, $\frac{\text{Fin normal force}}{qS}$

C_{hea}	fin moment coefficient measured about fin balance electrical axis which is not at the fin hinge axis, $\frac{\text{Fin moment}}{qS\bar{c}}$
C_h	fin hinge-moment coefficient, $C_{hea} + C_{NF} \frac{a}{\bar{c}}$
$\left. \begin{array}{l} \Delta C_m \\ \Delta C_h \\ \Delta C_{NF} \end{array} \right\}$	difference between value of coefficient at some fin-deflection angle and zero fin deflection
C_{PB}	missile base-pressure coefficient, $\frac{P_B - p}{q}$
A	maximum cross-sectional area of missile body, $\frac{\pi d^2}{4}$
a	distance between fin balance electrical axis and fin hinge axis
b	total fin span
c	local exposed-fin chord parallel to plane of symmetry
\bar{c}	mean aerodynamic chord of exposed fin, $\frac{2}{S} \int_0^{b/2} c^2 db$
d	maximum diameter of missile body, 1 caliber
ΔH	decrement in free-stream total pressure
M	Mach number
P_B	static pressure inside of open base of model
p	free-stream static pressure
q	free-stream dynamic pressure, $\frac{1}{2} \rho U^2$
R	free-stream Reynolds number, $\frac{\rho U \bar{d}}{\mu}$
r	radial distance from missile center line

S	exposed horizontal-fin area
U	free-stream velocity
α	angle of attack (see fig. 1)
ψ	complement of angle of attack, $90^\circ - \alpha$
β	angle of sideslip (see fig. 1)
ϕ	azimuth angle in plane normal to missile axis
δ_H	angle of horizontal-fin deflection (see fig. 1)
δ_V	angle of vertical-fin deflection (see fig. 1)
ρ	free-stream mass density
μ	absolute viscosity

MODEL AND APPARATUS

The model used in the present investigation was designed and constructed for subsonic tests in the Langley low-turbulence pressure tunnel described in references 1 and 2. Sketches of the model details are presented in figure 2 and photographs of the model mounted in the tunnel are shown in figure 3.

The body of the model was an assembled group of conical sections of turned aluminum alloy. The body of 5-inch maximum diameter and fineness ratio of 8.45 had a 31.5° nose section and a 4.5° boattail.

Four 60° triangular fins of double wedge section having the maximum thickness at 70 percent chord were mounted in cruciform at the base of the missile. Two of the diametrically opposed fins were constructed of aluminum alloy and were stationary at zero deflection angle; the other pair were made of steel and could be deflected. At zero fin deflection, there was a 0.026-inch gap between the body and the fins. A clearance gap of 0.021 inch around the fin pivot shaft allowed a leakage between the inside and outside of the model. This clearance hole was sealed when fins were removed for body-alone tests.

Total forces and moments were measured on the sting-mounted model by means of an internally located six-component, electrical strain-gage balance which was attachable to the model in two positions of roll so

that the adjustable fins could be tested in either the horizontal or the vertical plane. An additional strain-gage balance was mounted inside the boattail and attached to the interlocked movable fins to provide measurements of the fin normal force and hinge moments.

Static-pressure tubes for measuring base pressures were installed on the side of the sting, inside the model, approximately $3/8$ inch forward of the base. A rake of total pressure tubes was used to survey the model wake at a station coincident with the model base.

TESTS

The tests were made with the use of Freon-12 as a flow medium (ref. 2) through a Mach number range up to 0.88. The maximum Mach number at choke was approximately 0.92 with the model at an angle of attack of 0° . The stagnation pressure was somewhat below atmospheric and was adjusted to maintain about constant maximum aerodynamic loading; coincidentally, a nearly constant Reynolds number of 2.1×10^6 (based on maximum diameter of missile or 17.7×10^6 based on missile length) was maintained throughout the Mach number range.

Measurements were made at values of the Mach number of 0.50, 0.70, 0.80, and 0.88 through a range of angle of attack from -16° to 26° and a range of sideslip angles from -7° to 4° . For the missile with all fins removed, measurements were made of the normal and chord forces and the pitching moments. Normal- and chord-force coefficients were converted to lift and drag coefficients by the relation shown in section "Symbols." In order to explain the effect of the body flow on the fin, wake surveys were made at the base of the body for the missile without fins.

For the missile complete with fins, total forces and moments associated with the model reference axes and horizontal-fin normal forces and corresponding fin moments were measured for fin-deflection angles of 0° , -2° , -4° , and -6° with the vertical fins at zero deflection. With horizontal fins at zero deflection and vertical fins adjustable, total forces and moments were measured for vertical-fin roll deflections of $\pm 2^\circ$, $\pm 4^\circ$, $\pm 6^\circ$, and $+6^\circ$ upper fin with -2° lower fin.

A general lack of scatter in the data is an indication of the repeatability of the measurements. Flagged (⊙) and plain (○) symbols used in some cases indicate representative repeat measurements. Maximum variations in the various coefficients from the mean faired value in percent of the maximum value of the coefficient were about as follows: ± 3 for C_L , ± 1 for C_D , ± 1 for C_M , ± 1 for $C_{H_{ea}}$, and ± 2 for C_{N_F} .

CORRECTIONS

The usual blocking corrections described in reference 3 were applied to all force and moment coefficients, Mach numbers, and pressure data. The angle of attack was corrected for model-support deflection due to aerodynamic loading. The angle of attack was also corrected by the method of reference 4 for upwash induced by the tunnel wall. The longitudinal-force data were adjusted by an amount equal to the change in pressure force on the base that would be obtained by changing the measured base pressure to free-stream static pressure.

The coefficients of force, moment, and pressure as well as free-stream Mach numbers measured in Freon-12 were converted to corresponding coefficients and Mach numbers in air by the method of reference 2.

All forces, moments, and pressures were examined for sting tare effects by comparing data at three sting sizes and extrapolating to zero sting area. Only the drag, lift, and base pressures required tare corrections and these only for the case of the missile without fins.

INVESTIGATION OF SCALE EFFECT

Because the test Reynolds number was limited to a value well below the possible flight value, and, in particular, because the Reynolds number based on the cross-component of velocity was fairly low, the possibility was considered that the test results might be subject to considerable scale effect. It would be expected, however, on the basis of the data for yawed cylinders (ref. 5) shown in figure 4, that the model crossflow Reynolds number was sufficiently high to avoid subcritical flow conditions. As for the possible scale effect on the fins, it has been shown (ref. 6) that the aerodynamic characteristics of some sharp-edge airfoils are decidedly nonlinear at low Reynolds numbers and at low angles of attack but become linear as the Reynolds number is increased; the same investigation showed that roughness largely eliminated the nonlinearities at low Reynolds numbers and suggested the possibility that roughness should be used on the missile fins.

In order to make certain that the values of the aerodynamic coefficients at some flight Reynolds number would not be appreciably different from the values obtained in the test, the complete missile was tested with fins and body rough to induce leading-edge transition, the essential characteristic of high Reynolds number flow. The body roughness consisted of four full-length longitudinal bands 1/2 inch wide located midway between the fins and two 1-inch bands around the body circumference, one at the nose and the other at the station of maximum diameter. The

roughness on the fins was a 1/4-inch band near the leading edge of both surfaces of each fin. The roughness used in all cases was 0.010- to 0.012-inch carborundum blown on shellac stripes.

As shown by the data in figures 5 and 6, the addition of roughness did not appreciably affect the aerodynamic characteristics of the fins or the complete missile. For convenience in the test procedure, the tests on stability and control were made with the body smooth and the fins rough.

RESULTS

A list of the basic data obtained in these tests is shown indexed to configuration and figure number in table I.

Pitching and yawing moments are presented as measured about a point 6.15 calibers from the model nose, which was the electrical axis of the balance. (See fig. 2(a).)

The base pressure coefficients are not presented for other than the body-alone case because of leakage around the fin pivot shaft.

DISCUSSION

Body Alone

Forces and moments.- The longitudinal-force and moment coefficients for the missile without fins are shown in figure 7. Qualitatively, the increase in value of the coefficients with Mach number agreed with the usual trend due to subsonic compressibility effects. The increase of lift-curve slope with angle of attack is similar to the trend predicted by body theory.

Wake-flow surveys.- Contours of total-pressure loss coefficients as measured at the model base are shown in figure 8 for the body without fins at three angles of attack (3.5° , 10° , and 20°) and at Mach numbers of 0.5 and 0.88. It will be noted from figure 8 that the wake size increases with angle of attack and, at the highest angle of attack, the wake size increases appreciably with Mach number. At the higher angles of attack, a characteristic of the wake typical of slender bodies is the development of regions of large loss and thus low velocities at azimuth angles of about $\pm 16^\circ$ whereas between the two regions a low-loss region exists. This type of flow probably indicates the presence of vortices such as were investigated in reference 7. The rapid changes of velocity for a

fin rolling through the wake region might be expected to have important effects on the fin performance.

Fin Forces and Moments

Unyawed condition.- The variation of normal-force coefficient on the horizontal fins was nonlinear with δ_H (fig. 9(a)) due in part at least to the usual effects of localized regions of leading-edge separation on thin swept wings. The increment of normal-force coefficient produced by the deflection of the fin from 0° to -6° does not change much with M or α as shown in figure 9(b).

The curves of fin hinge-moment coefficient C_{H_F} in figure 10(b) were obtained by transferring the values of the moments measured about the electrical axis of the strain-gage balance (fig. 10(a)) by the use of faired values of the normal force. The accuracy of the C_{H_F} curves is estimated to be ± 0.003 and, therefore, conclusions on the variation of C_{H_F} that require greater accuracy are not justified; however, some general observations may be made. The noticeable changes in the slope of C_{H_F} against α at α equal to about $\pm 8^\circ$ are due to changes in the center-of-pressure position inasmuch as the normal-force coefficient in this range of angle of attack is linear with angle of attack. The hinge-moment coefficient was, in general, nonlinear with both δ_H and α . Average values of the rate of change of hinge-moment coefficient with δ_H (fig. 10(c)) and α (fig. 10(b)) decrease with increasing Mach number.

Sideslip.- Although the hinge-moment and the fin normal-force coefficients vary rather irregularly with β at high values of α (fig. 11), a general effect of increasing the sideslip is to decrease these coefficients. The irregular results at high angles of attack are due possibly to dissymmetry in the wake flow which at those angles can easily result from very small surface irregularities.

Longitudinal Stability and Control Characteristics

Unyawed condition.- From figure 12, it may be seen that the lift coefficient is not affected much by Mach number. The nonlinear lift-coefficient variation with δ_H is probably due to the effect of δ_H on the fin normal-force coefficient inasmuch as the finned missile had a lift of about three times the body-alone lift. The increasing slope of the lift curves with increasing α results partially from nonlinear lift contributions of the body and may also result from the leading-edge vortex effect on the fins. It may be of interest to note that a deflection of the fin through a given angle changes the lift about two-thirds as much as an equal change of angle of attack.

~~CONFIDENTIAL~~

The pitching-moment coefficient (fig. 13) was found to be quite nonlinear with α and to some extent with δ_H . Near $\alpha = 0$ the value of the slope of C_m with α at constant δ_H was nearly zero and therefore the moment-measuring axis was near the aerodynamic center of the missile.

In order to discuss the missile stability and control characteristics without limiting the observations to a specific center-of-gravity position, these characteristics can be discussed in terms of the variation of the center-of-gravity positions required for trim and neutral stability through the range of angle of attack and fin deflection. The center of gravity for trim at any condition of α , δ_H , and Mach number investigated is the center of pressure for the same set of conditions. Such center-of-pressure positions may be obtained from plots of C_m against C_N shown in figure 14 (where the center of pressure is C_m/C_N). The center-of-gravity position for neutral longitudinal stability combined with trim is the neutral point corresponding to $\left(\frac{\partial C_m}{\partial C_N} \right)_{\delta_H \text{ constant}} = \frac{C_m}{C_N}$. All combina-

tions of C_m and C_N that fall on the same line drawn from the origin in figure 14 have the same center of pressure. For convenience, the value of the center of pressure for a given line drawn from the origin may be read from the semicircular scale superimposed in figure 14. A neutral point for a given fin deflection can be found in figure 14 by drawing a line from the origin tangent to the curve of C_m against C_N at constant δ_H . The slope of the line from the origin gives the position of the neutral point and the point of tangency gives the corresponding angle of attack. Because of the nonlinearity of the normal-force and moment characteristics, the neutral point changes with angle of attack.

The region of center-of-pressure travel through the range of horizontal-fin deflections from -6° to 6° is shown in figure 15 for the measured range of angles of attack; this region did not change much from a Mach number of 0.5 to 0.88. The travel of center of pressure becomes small at the high angles of attack; for example, at $\alpha = 16^\circ$ the travel is between 5.6 and 6.5 calibers from the nose; hence, any longer travel of the center of gravity can not be trimmed.

The variation of neutral point with angle of attack is also shown in figure 15 for Mach numbers of 0.5 and 0.88, comparison of which indicates that the variation is small with Mach number. The variation of the neutral point with angle of attack was about 1 caliber through the range of angle of attack for which the neutral point could be determined. Stable and trimmed flight is obtained, of course, if the center of gravity is ahead of the neutral point and behind the center-of-pressure boundary

~~CONFIDENTIAL~~

for trim at maximum deflection of the fin. At a Mach number of 0.88, stable flight cannot be maintained simultaneously with trim at angles of attack greater than 17° for any center of gravity without larger fin deflections or the use of some auxiliary device for stability and control such as jet vanes; at a Mach number of 0.5, this angle-of-attack range is extended to 20° .

The drag coefficients for the same attitudes and flight conditions as discussed for control and stability are shown in figure 16.

Sideslip.- Lift, pitching-moment and drag coefficients are presented in figures 17, 18, and 19, respectively, for several roll deflections of the vertical fins. At low angles of attack, an increase in sideslip up to -7° (fig. 18) does not appreciably affect the longitudinal stability; in the angle-of-attack range from 15° to 20° , however, an increase in sideslip angle is obviously destabilizing. These observations remain unchanged throughout the Mach number range and through the fin roll-deflection range of 0° to $\pm 6^\circ$.

Lateral Stability and Control Characteristics

Unyawed condition.- The effectiveness of the fin for producing a rolling-moment coefficient increases slightly with angle of attack but does not change appreciably with Mach number as shown in figure 20(a). The greater effectiveness of the fins in roll at the higher angles of attack (near 20°) occurred primarily at the low angles of fin deflection. The crossover of rolling-moment coefficient at the low deflection and the high angles of attack and high Mach number is probably the result of an erratic body-wake effect on the fin. As may be seen from figures 20(b) and 20(c), the effects of fins deflected for roll are small on the side-force coefficient and yawing-moment coefficient.

Sideslip condition.- Figure 21(a) indicates that the directional stability $\partial C_n / \partial \beta$ decreases at the higher angles of attack. At fin deflections of zero, the data indicated that sideslip causes no rolling moment for the test angles of attack of 0° and about 16° ; however, at angles of attack between 0° and 16° , small rolling moments may exist in a direction opposite to the rolling moments measured at higher angles of attack due to a positive dihedral effect of the horizontal fins. For angles of attack greater than 16° the rolling moment increases rapidly with sideslip angle; this result at the high angles of attack is to be expected for the upper fin moving into the body wake and losing effectiveness in counteracting the rolling moment produced by the lower fin. At the highest angle of attack tested, the rolling moment at a Mach number of 0.5 could be trimmed out with a roll deflection of 6° for values of the sideslip angle between $\pm 6.5^\circ$ and at a Mach number of 0.88 the range of sideslip angles for trim was reduced to $\pm 3^\circ$. This effect of

Mach number is consistent with the wake surveys where at the higher Mach number a larger wake would envelop the upper fin at the high angles of attack for the yawed condition.

The data presented in figure 21(c) are the lateral-force and moment coefficients for a combination of roll deflection and yaw deflection of the vertical fins. In order to determine the effect on the roll effectiveness of superimposing a yaw deflection on the vertical fins already deflected for roll, compare rolling-moment coefficients at a Mach number of 0.88 for a roll deflection of 4° (fig. 21(b)) and a combination of 6° upper fin and 2° lower fin (fig. 21(c)) which geometrically corresponds to 4° of roll and 2° of yaw. It may be seen from this comparison that roll effectiveness is very little affected by the addition of a yaw deflection at least for small deflections and for the range of angle of attack and sideslip tested.

CONCLUSIONS

Static stability and control tests have been made of a model of a wingless fin-controlled missile and the following conclusions are presented for a Mach number range of 0.50 to 0.88 and a fin-deflection range up to 6° :

1. Trimmed stable longitudinal flight cannot be maintained with fin deflection limited to a maximum of 6° , for angles of attack greater than 17° at a Mach number of 0.88 or angles of attack greater than 20° for a Mach number of 0.50 for any center-of-gravity location without the use of some auxiliary stability or control device such as jet vanes.
2. Mach number affected the position of the neutral points only slightly. Through the angle-of-attack range for which the neutral point could be determined, the neutral point varied over a distance of about 1 caliber. The centers of pressure were not appreciably affected by Mach number.
3. Up to an angle of attack of 15° , the longitudinal stability was little affected by sideslip up to angles of sideslip of 7° . In the angle-of-attack range from 15° to 21° , an increase in sideslip resulted in decreased longitudinal stability.
4. At the highest angle of attack tested (26.5°) and with a roll deflection of the fins of 6° , the rolling moment could be trimmed out up to angles of sideslip of 6.5° at a Mach number of 0.50; this range was reduced to 3° at a Mach number of 0.88. At lower angles of attack, the missile could be trimmed in roll to higher angles of sideslip.

~~CONFIDENTIAL~~

5. Both the horizontal-fin normal-force and hinge-moment coefficients were somewhat nonlinear with angle of attack and fin deflection.

6. As the Mach number was increased the magnitudes of slopes of fin hinge moments with angle of attack and fin deflection ($\partial C_{H_F} / \partial \alpha$ and $\partial C_{H_F} / \partial \delta$, respectively) were appreciably reduced.

7. The general effect of increasing the angle of sideslip was to decrease the horizontal-fin coefficients of normal force and hinge moment.

Langley Aeronautical Laboratory,
National Advisory Committee for Aeronautics,
Langley Field, Va., October 6, 1953.

REFERENCES

1. Von Doenhoff, Albert E., and Abbott, Frank T., Jr.: The Langley Two-Dimensional Low-Turbulence Pressure Tunnel. NACA TN 1283, 1947.
2. Von Doenhoff, Albert E., and Braslow, Albert L.: Studies of the Use of Freon-12 As a Testing Medium in the Langley Low-Turbulence Pressure Tunnel. NACA RM L51L11, 1951.
3. Herriot, John G.: Blockage Corrections for Three-Dimensional-Flow Closed-Throat Wind Tunnels, With Consideration of the Effect of Compressibility. NACA Rep. 995, 1950. (Supersedes NACA RM A7B28.)
4. Katzoff, S., and Hannah, Margery E.: Calculation of Tunnel-Induced Upwash Velocities for Swept and Yawed Wings. NACA TN 1748, 1948.
5. Bursnall, William J., and Loftin, Laurence K., Jr.: Experimental Investigation of the Pressure Distribution About a Yawed Circular Cylinder in the Critical Reynolds Number Range. NACA TN 2463, 1951.
6. Schwartzberg, Milton A.: Effects of Roughness and Reynolds Number on the Nonlinear Lift Characteristics of a Wing With Modified Hexagonal Airfoil Sections. NACA RM L52L26a, 1953.
7. Spahr, J. Richard, and Dickey, Robert R.: Wind-Tunnel Investigation of the Vortex Wake and Downwash Field Behind Triangular Wings and Wing-Body Combinations at Supersonic Speeds. NACA RM A53D10, 1953.

~~CONFIDENTIAL~~

TABLE I.- TABLE OF RESULTS

Configuration	Type of data	Range of angles of attack and yaw, deg	Fin deflections		Figure
			δ_H , deg	δ_V , deg	
Missile without fins	Longitudinal forces and moments and base pressure	$\alpha = -16$ to 26 $\beta = 0$	None	None	7
	Flow surveys at model base	$\alpha = 3.5, 10, 20$ $\beta = 0$	None	None	8
Missile with fins	Fin forces and moments	$\alpha = -16$ to 26 $\beta = 0$	0 to -6	0	9 and 10
		$\beta = -7$ to 4 $\alpha = 0, 16, 21, 26$	0	0	11
	Longitudinal forces and moments	$\alpha = -16$ to 26 $\beta = 0$	0 to -6	0	12 (C_L) 13 (C_m) 14 (C_m) and (C_N) 15 (centers of pressure and neutral points) 16 (C_D)
		$\beta = -7$ to 4 $\alpha = 0, 16, 21, 26$	0	Roll deflection 0, ± 4 , ± 6	17 (C_L) 18 (C_m) 19 (C_D)
	Lateral forces and moments	$\alpha = -16$ to 26 $\beta = 0$	0	0, ± 2 , ± 4 , ± 6	20
		$\beta = -7$ to 4 $\alpha = 0, 16, 21, 27$	0	0, ± 4 , ± 6	21(a) and 21(b)
		$\beta = -7$ to -4 $\alpha = 16, 21, 27$	0	+6 top -2 bottom	21(c)

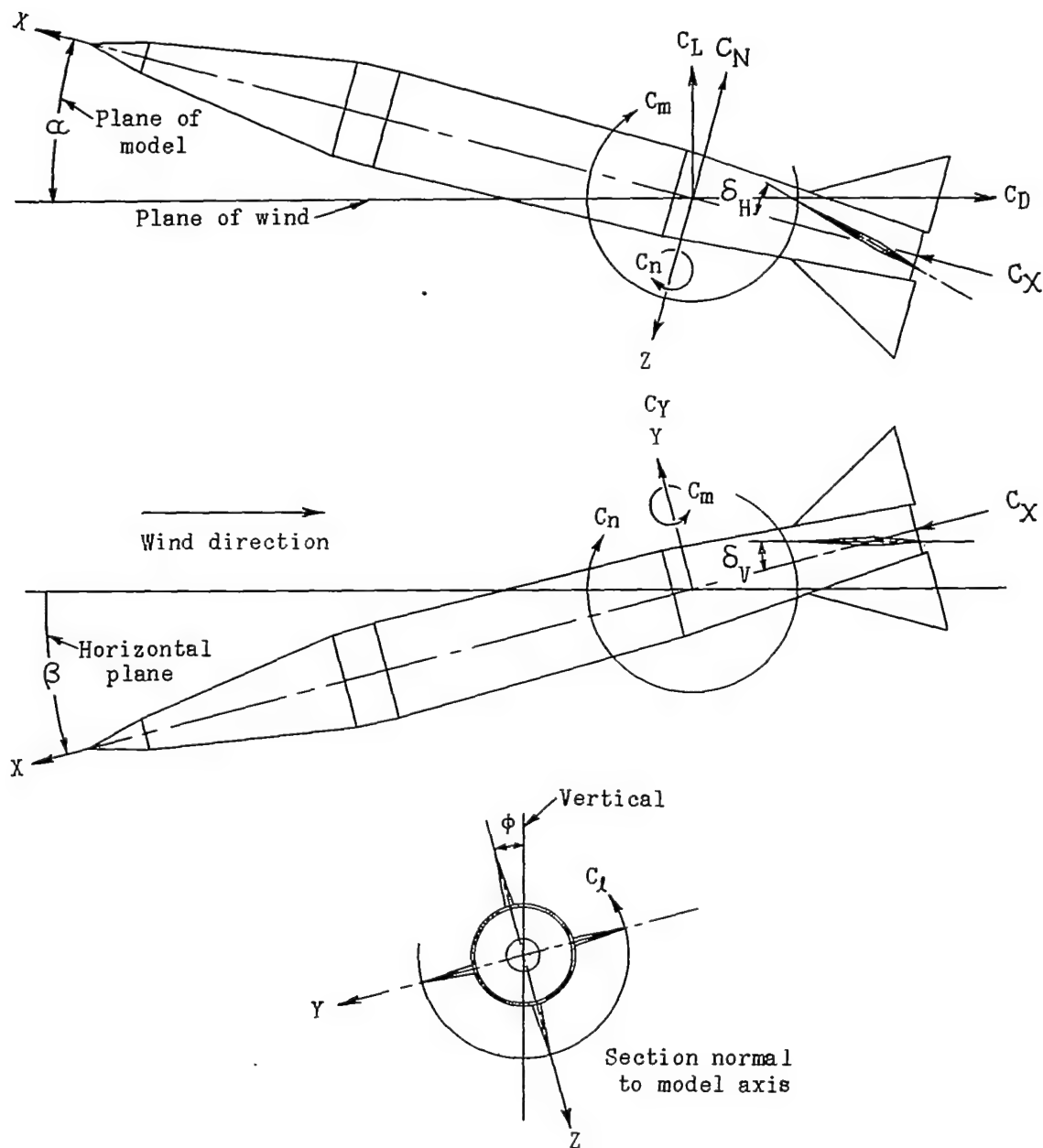
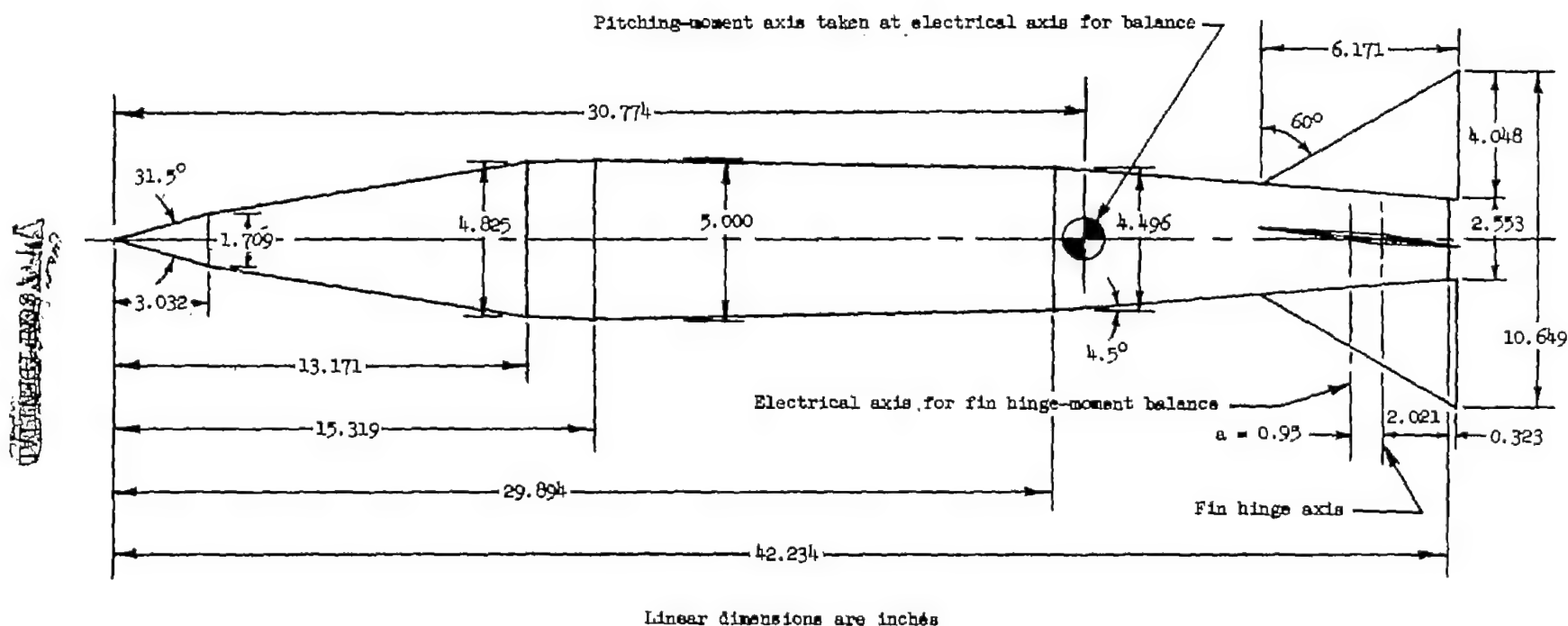
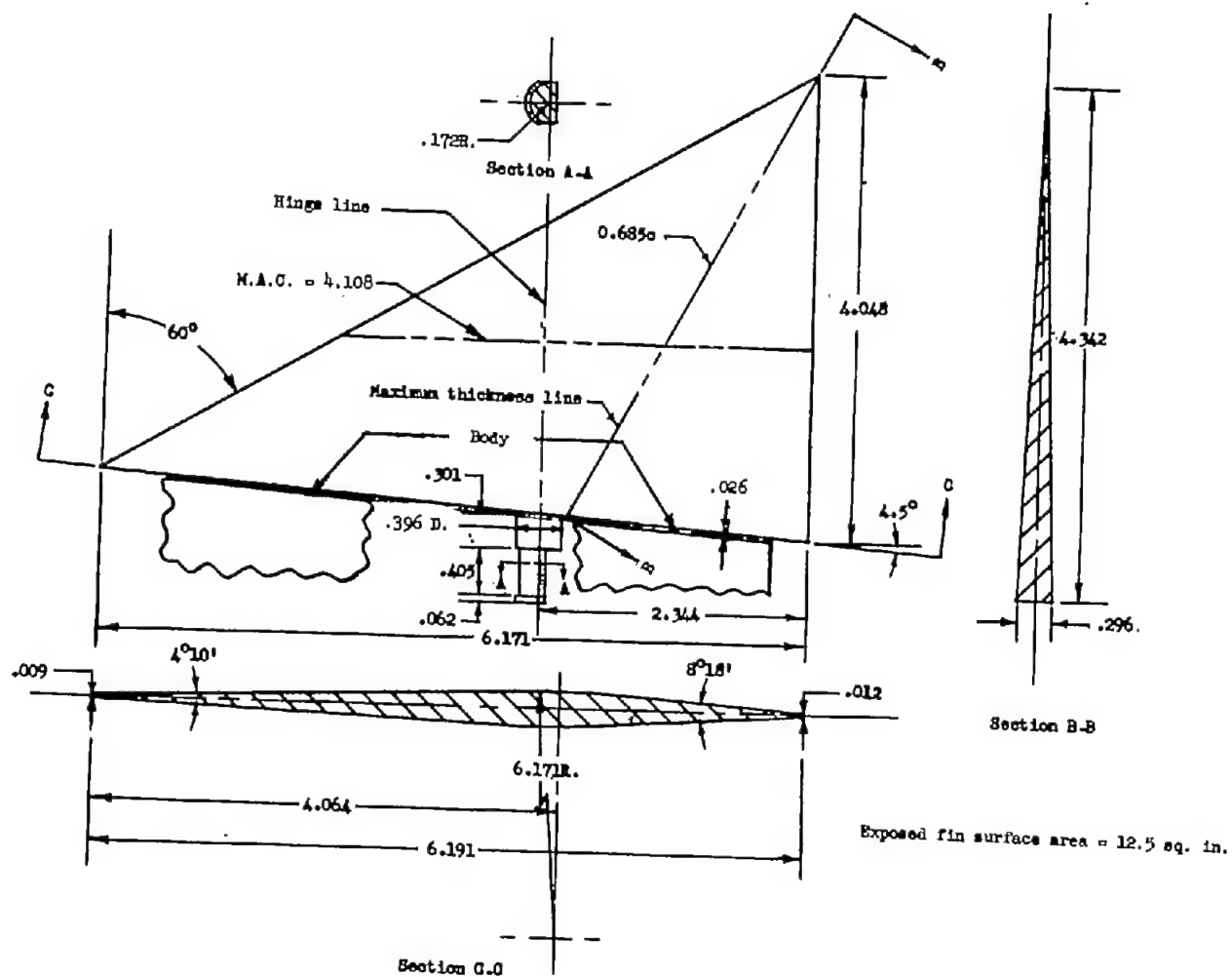


Figure 1.- The model system of axes. Arrows indicate positive directions of moments and forces.



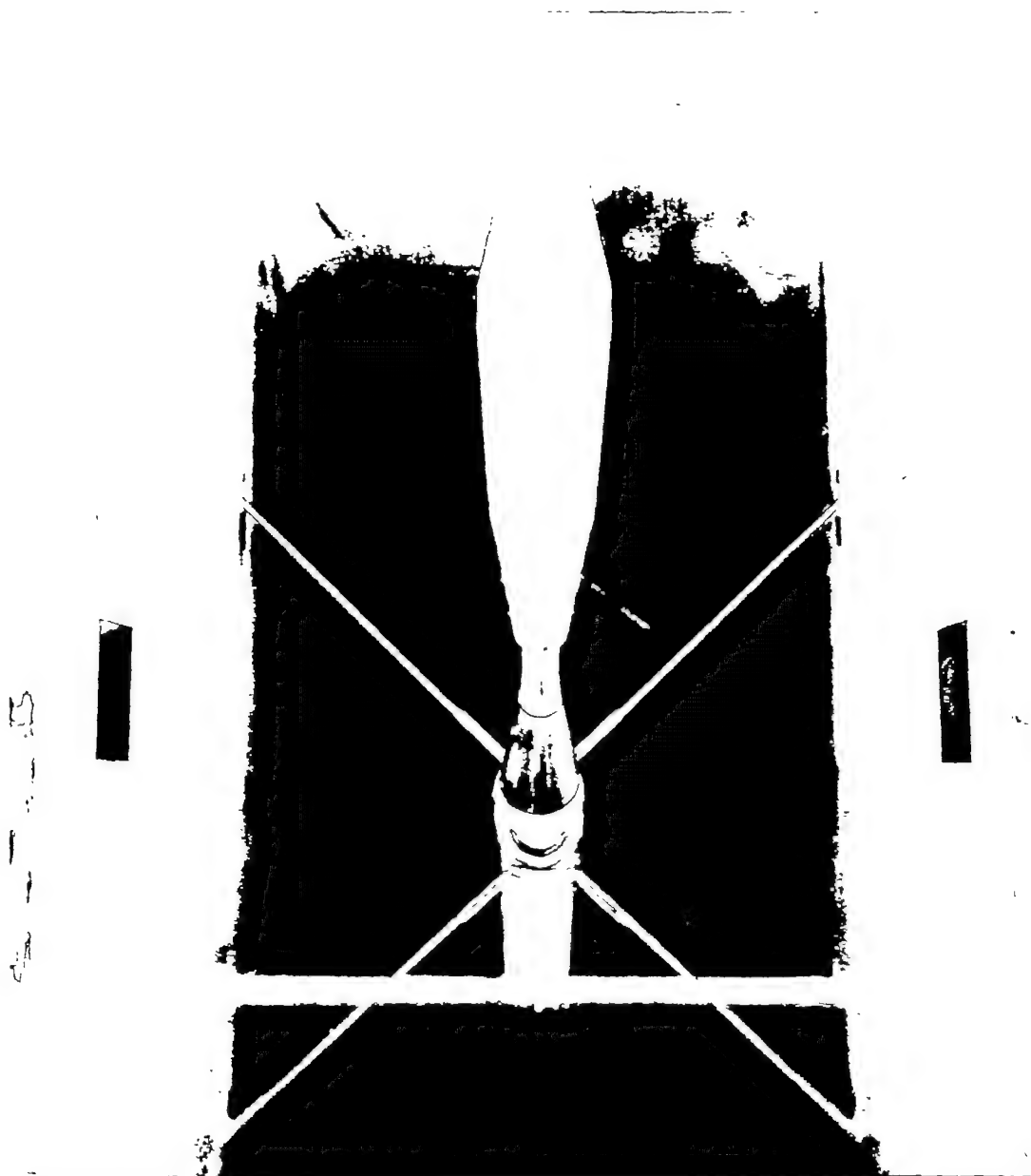
(a) Complete missile model.

Figure 2.- Diagram of a wingless fin-controlled missile. Linear dimensions are in inches.



(b) Fin details.

Figure 2.- Concluded.



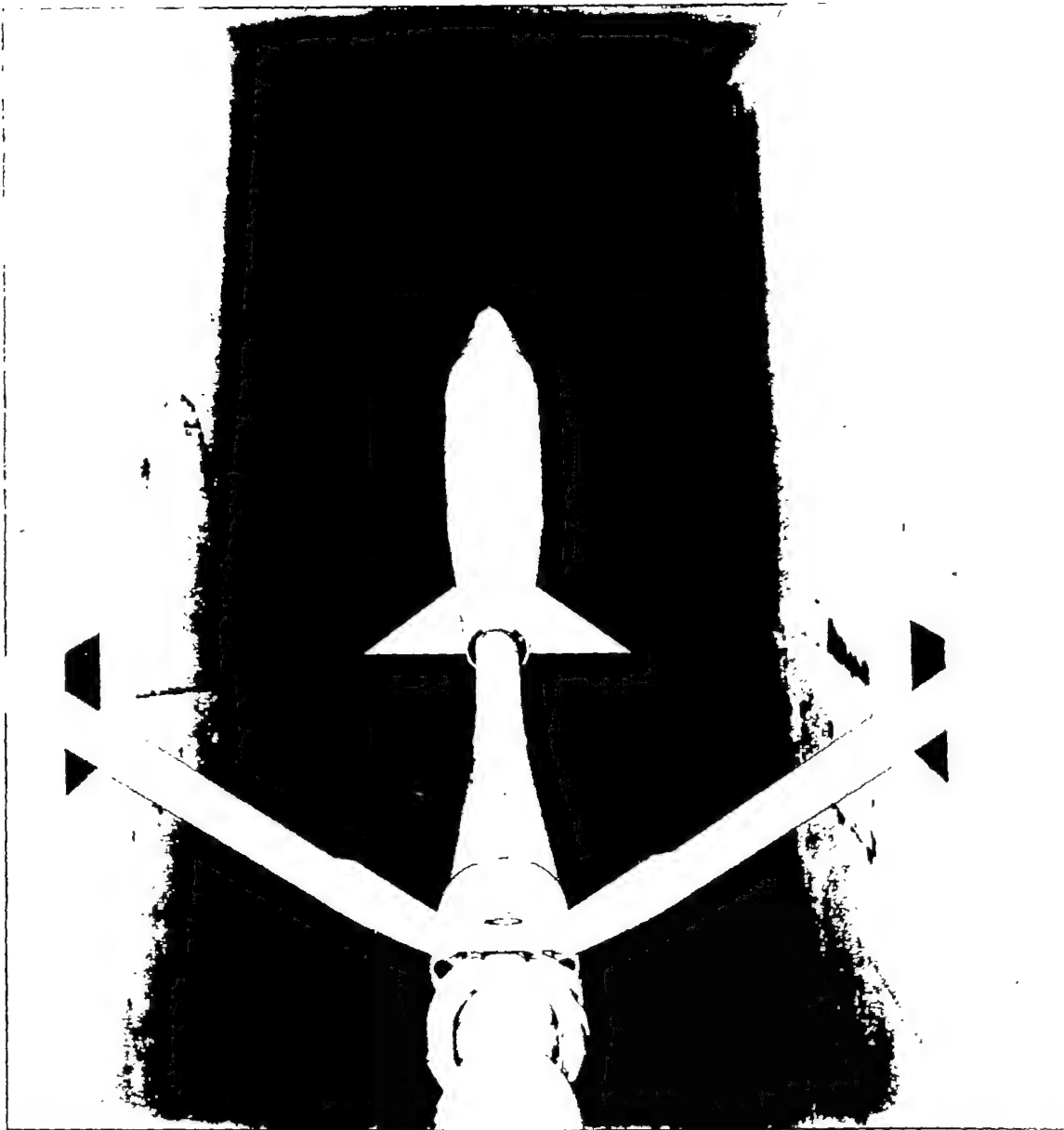
(a) Front view.

L-77849

Figure 3.- Photographs of a model of a wingless fin-controlled missile mounted on the sting balance in the Langley low-turbulence pressure tunnel.

~~CONFIDENTIAL~~

NACA RM L53J06



(b) Rear view.

L-77850

Figure 3.- Concluded.

~~CONFIDENTIAL~~

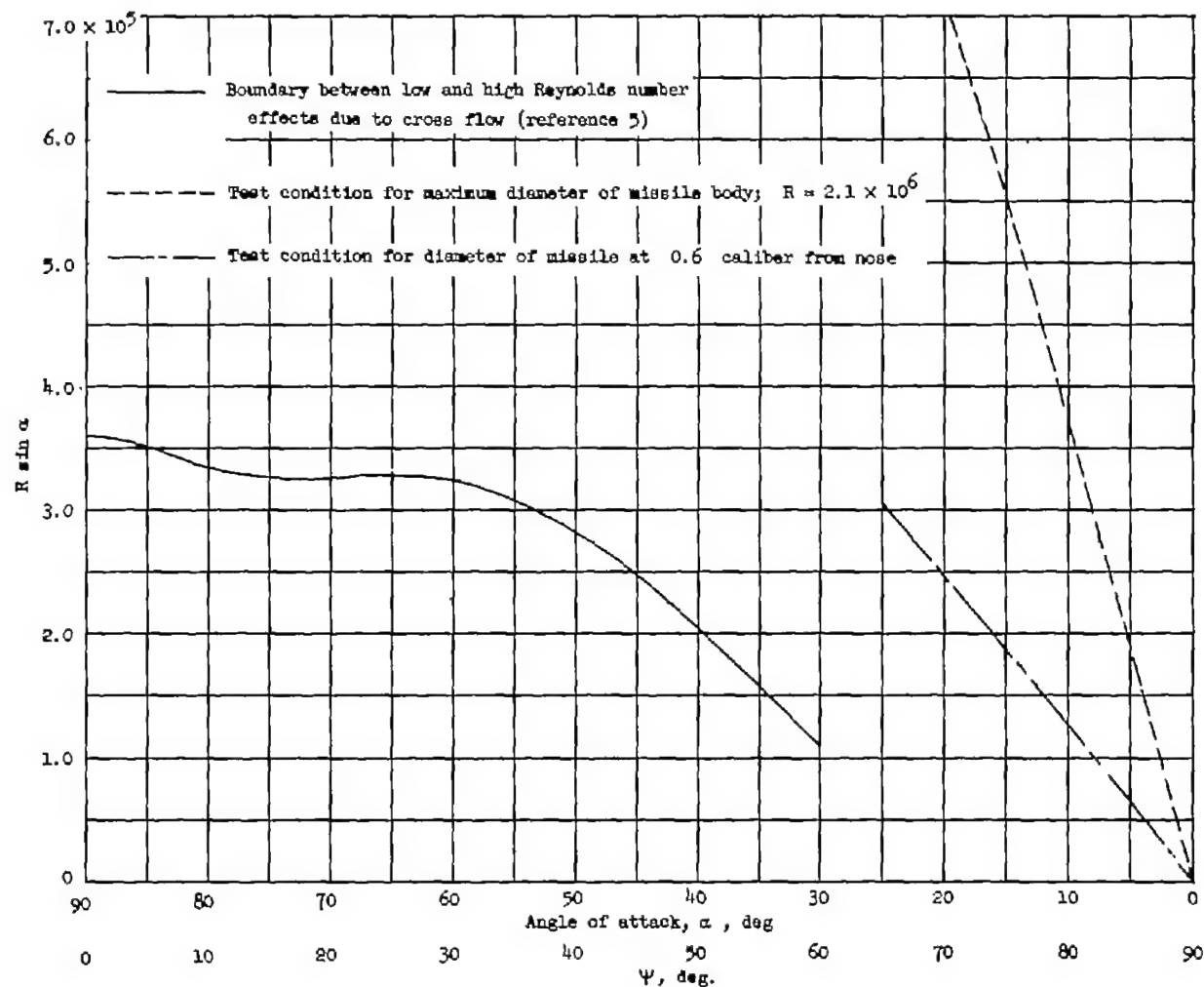


Figure 4.- An estimate of adverse low Reynolds number effects on the body of a wingless fin-controlled missile due to crossflow at angles of attack. The values of ψ are from reference 5.

CONFIDENTIAL

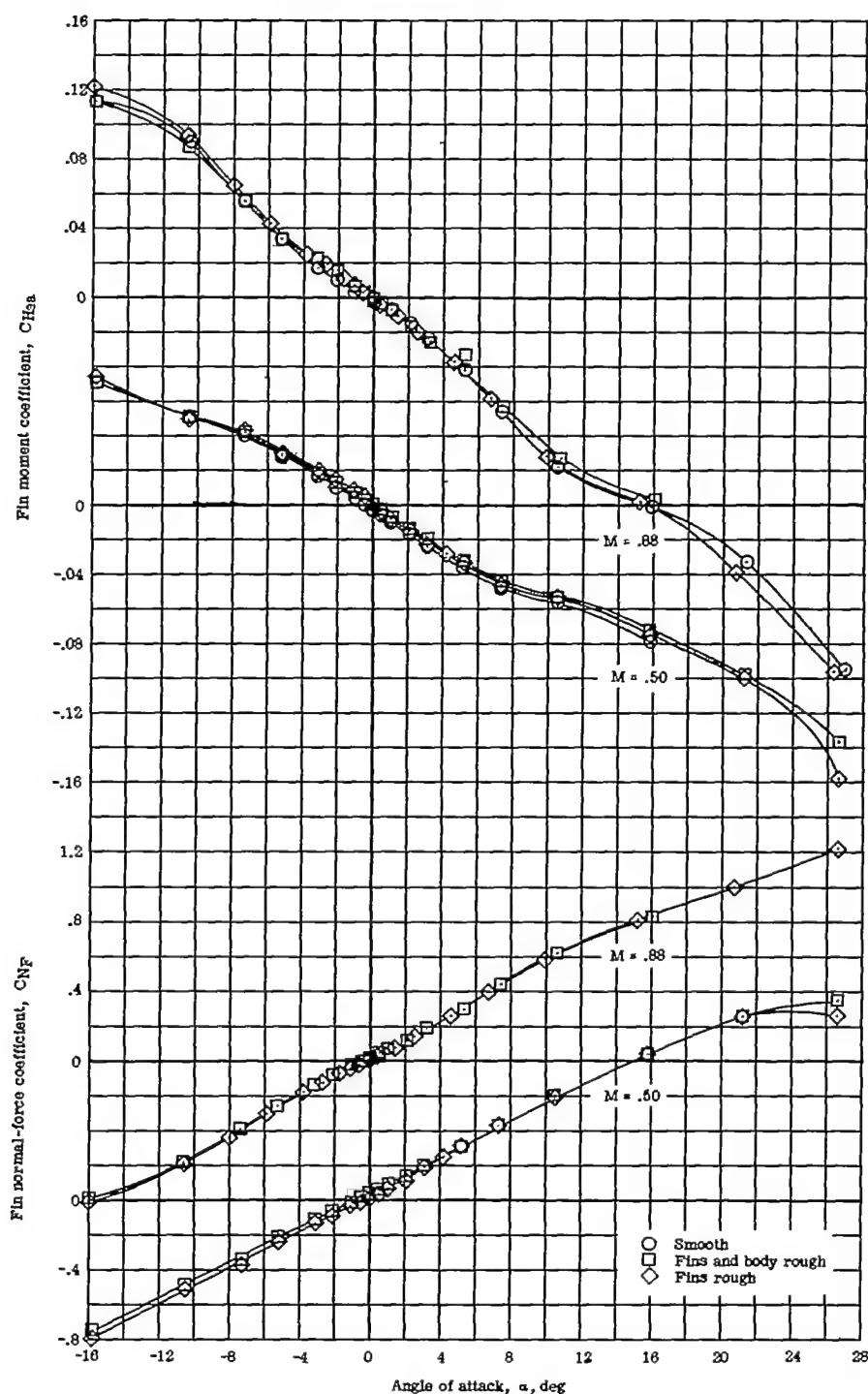


Figure 5.- A comparison of the effects of surface roughness on the variation of horizontal-fin force and moment coefficients with angle of attack for a wingless fin-controlled missile model at two Mach numbers. $\beta = 0^\circ$; $\delta_H = 0^\circ$; $\delta_V = 0^\circ$.

CONFIDENTIAL

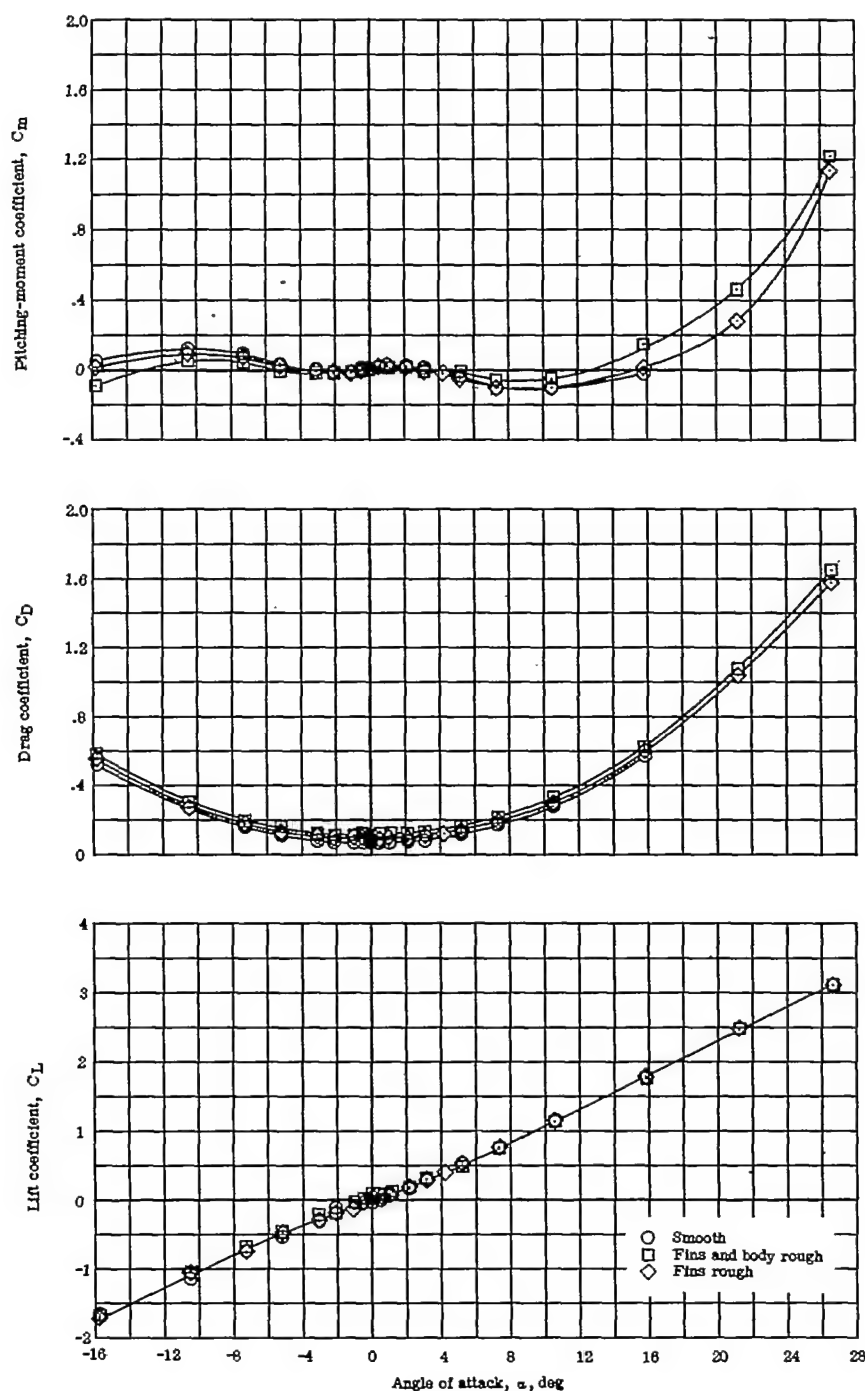
(a) $M = 0.50$.

Figure 6.- A comparison of the effects of surface roughness on the variation of longitudinal-force and moment coefficients with angle of attack for a wingless fin-controlled missile model at two Mach numbers.

$\beta = 0^\circ$; $\delta_H = 0^\circ$; $\delta_V = 0^\circ$.

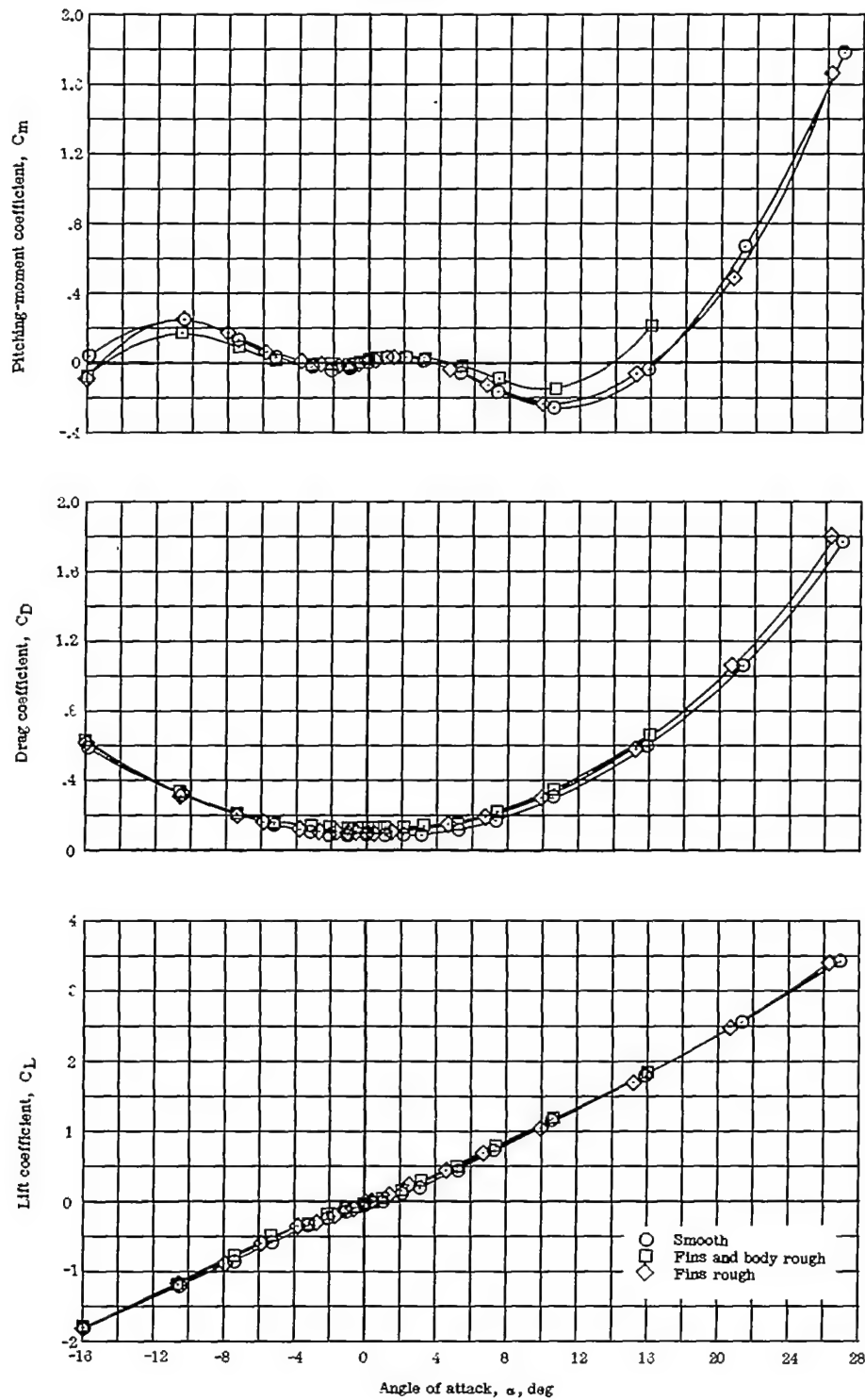
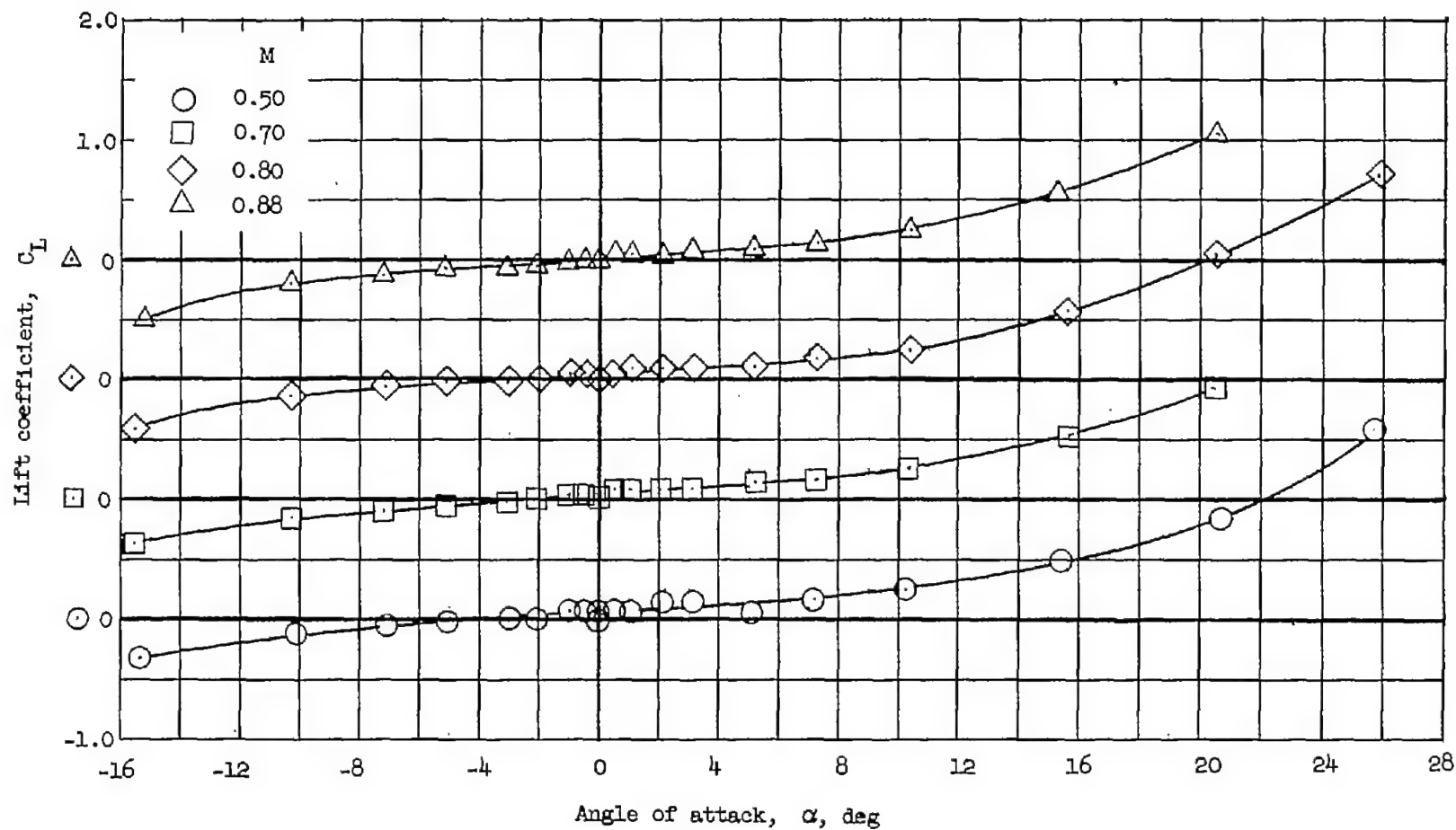
~~CONFIDENTIAL~~(b) $M = 0.88$.

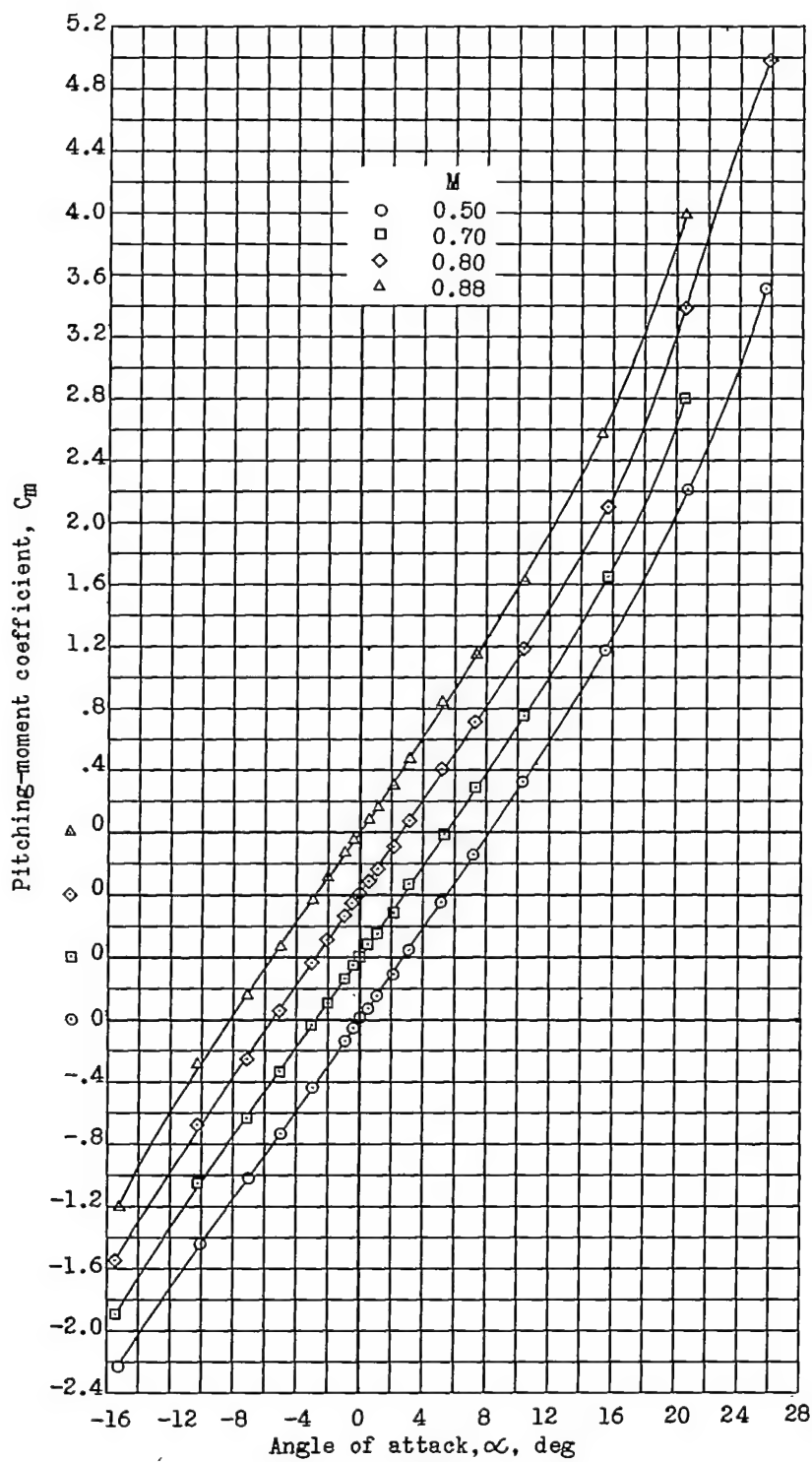
Figure 6.- Concluded.

~~CONFIDENTIAL~~



(a) Lift.

Figure 7.- Lift, pitching-moment, base-pressure, and drag variations for the body of a wingless fin-controlled missile model at four Mach numbers. Fins removed.

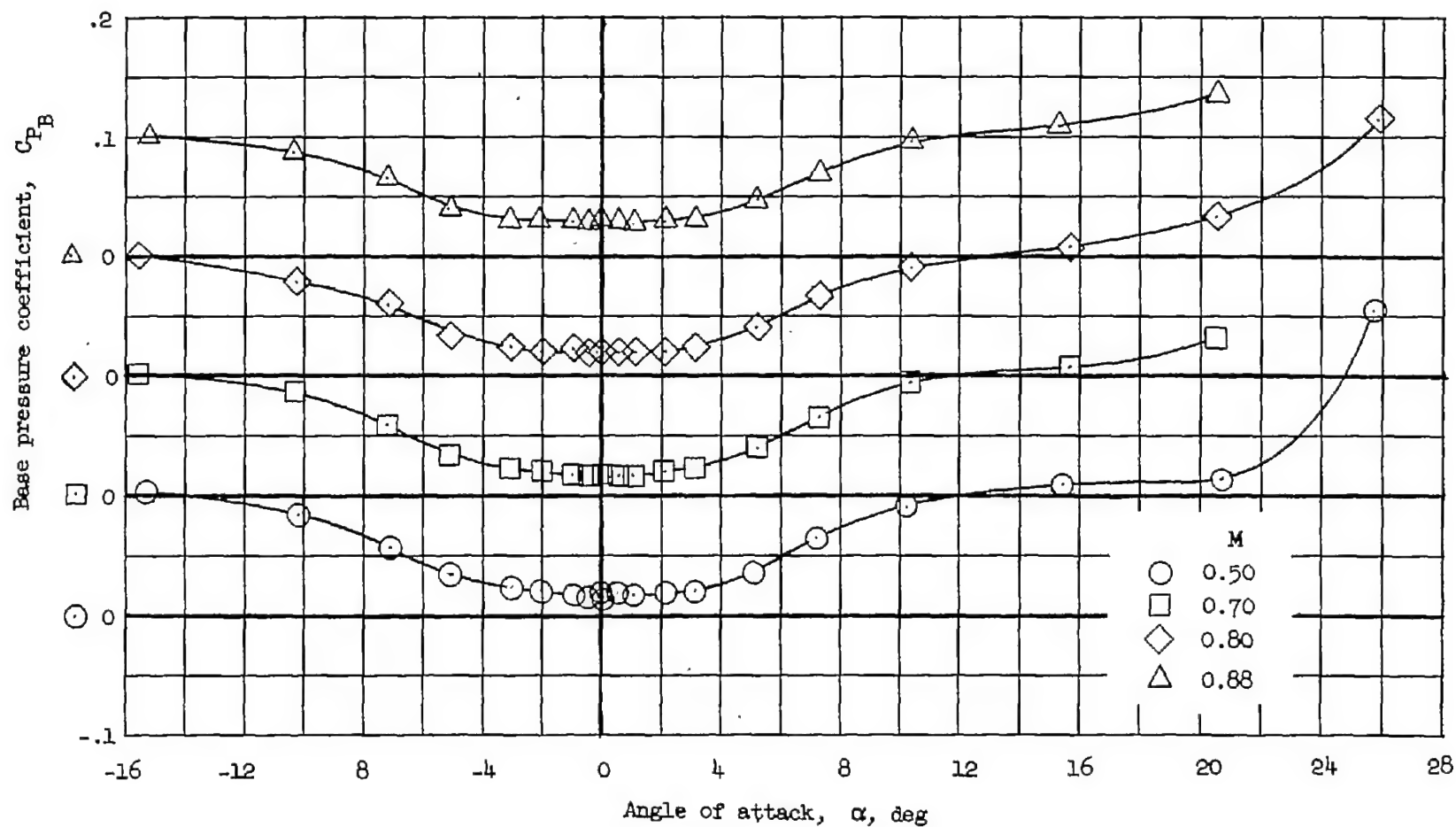
~~CONFIDENTIAL~~

(b) Pitching moment.

Figure 7.- Continued.

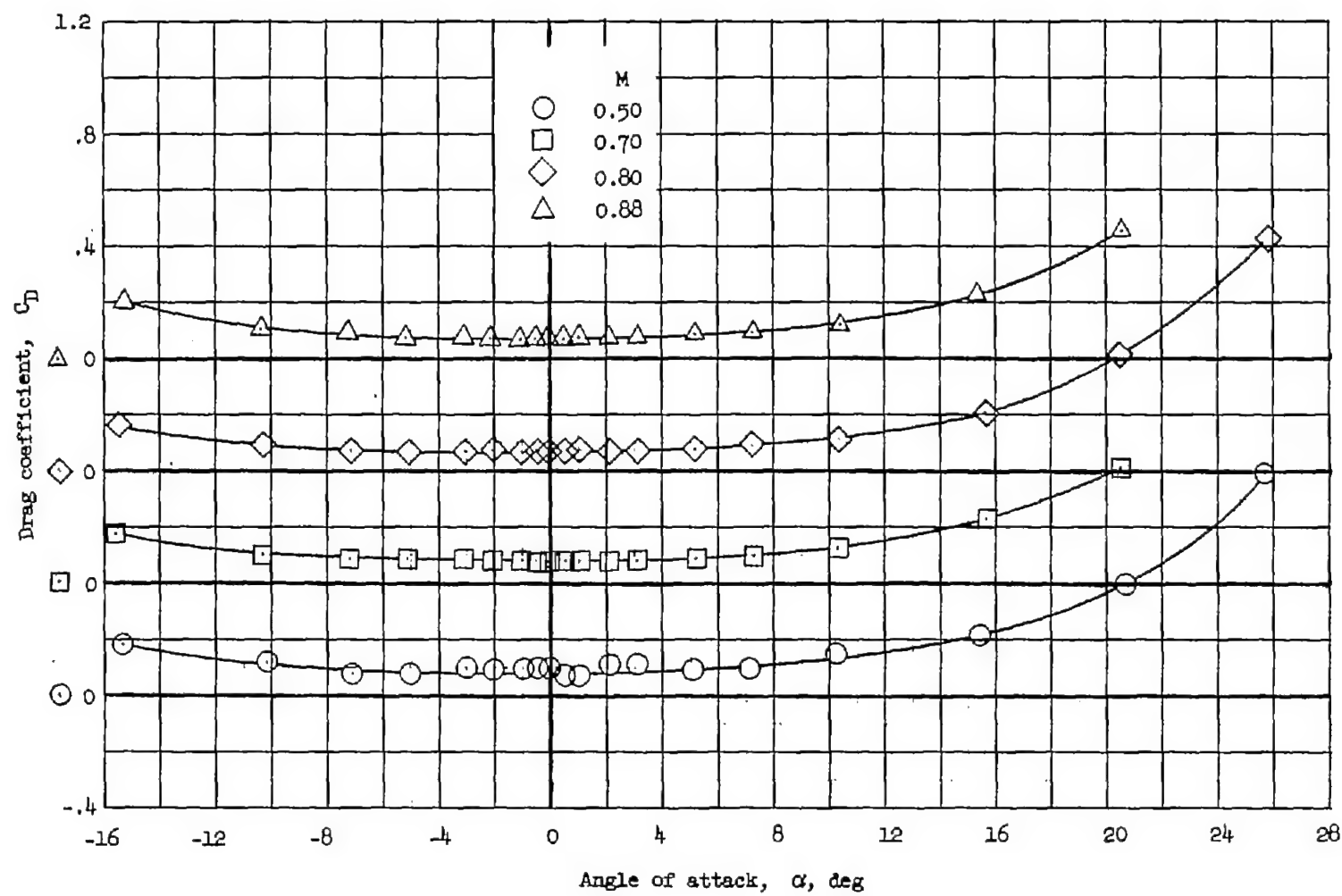
~~CONFIDENTIAL~~

CONFIDENTIAL



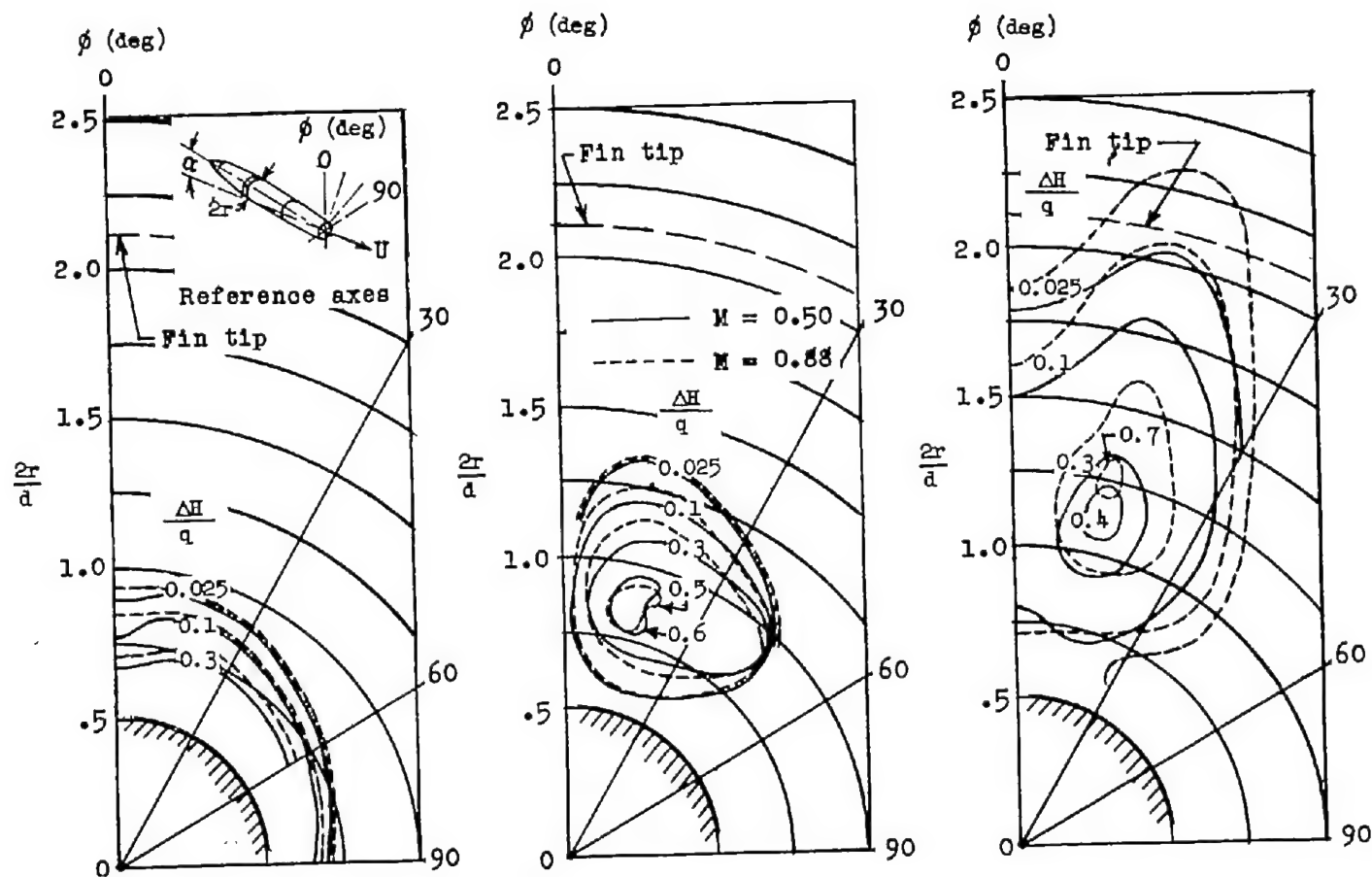
(c) Base pressure.

Figure 7.- Continued.



(d) Drag.

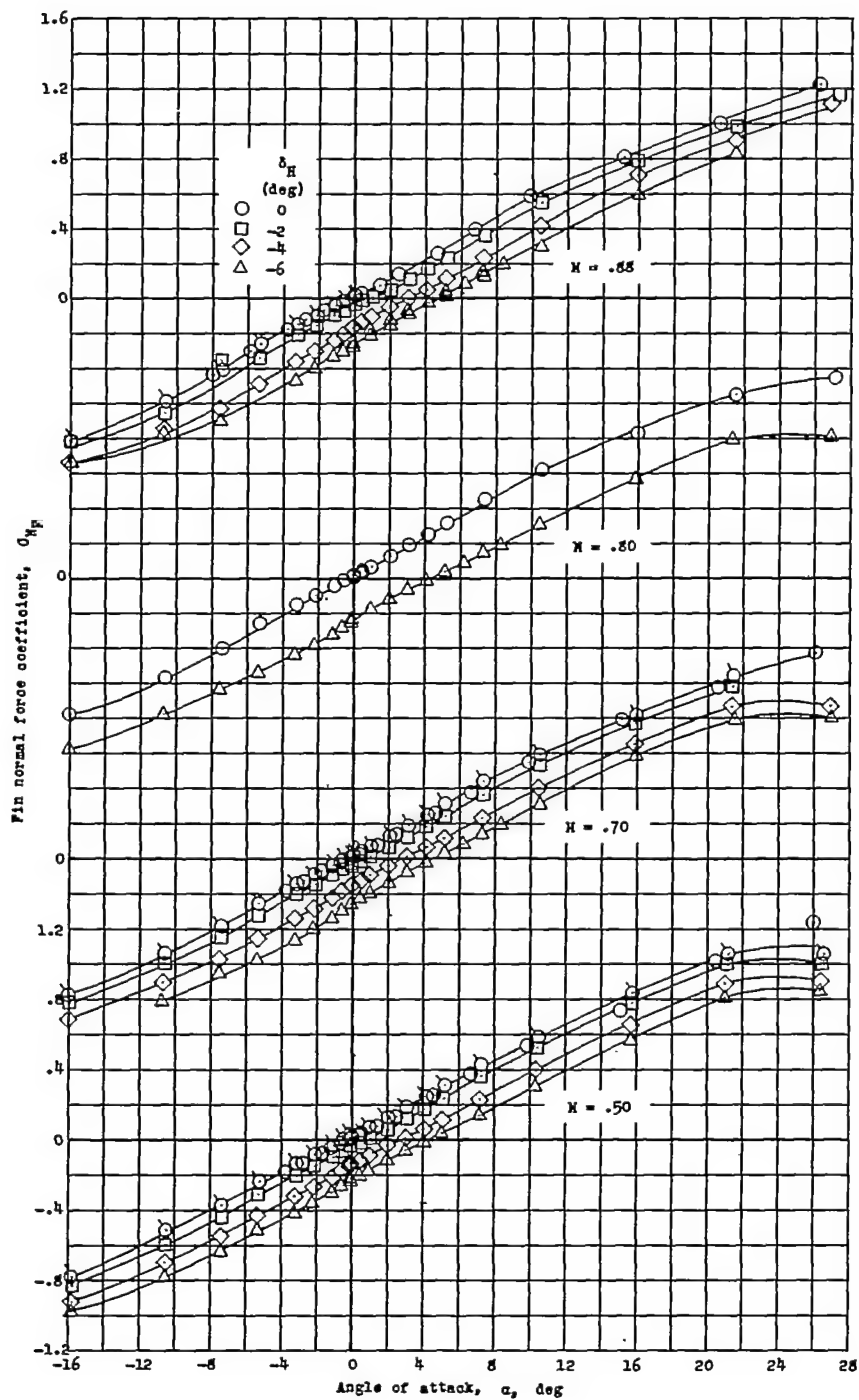
Figure 7.- Concluded.



(a) Angle of attack α , 3.5° . (b) Angle of attack α , 10° . (c) Angle of attack α , 20° .

Figure 8.- Total-pressure-loss survey at the base of the body for a wingless fin-controlled missile model at two Mach numbers and three angles of attack. Fins removed.

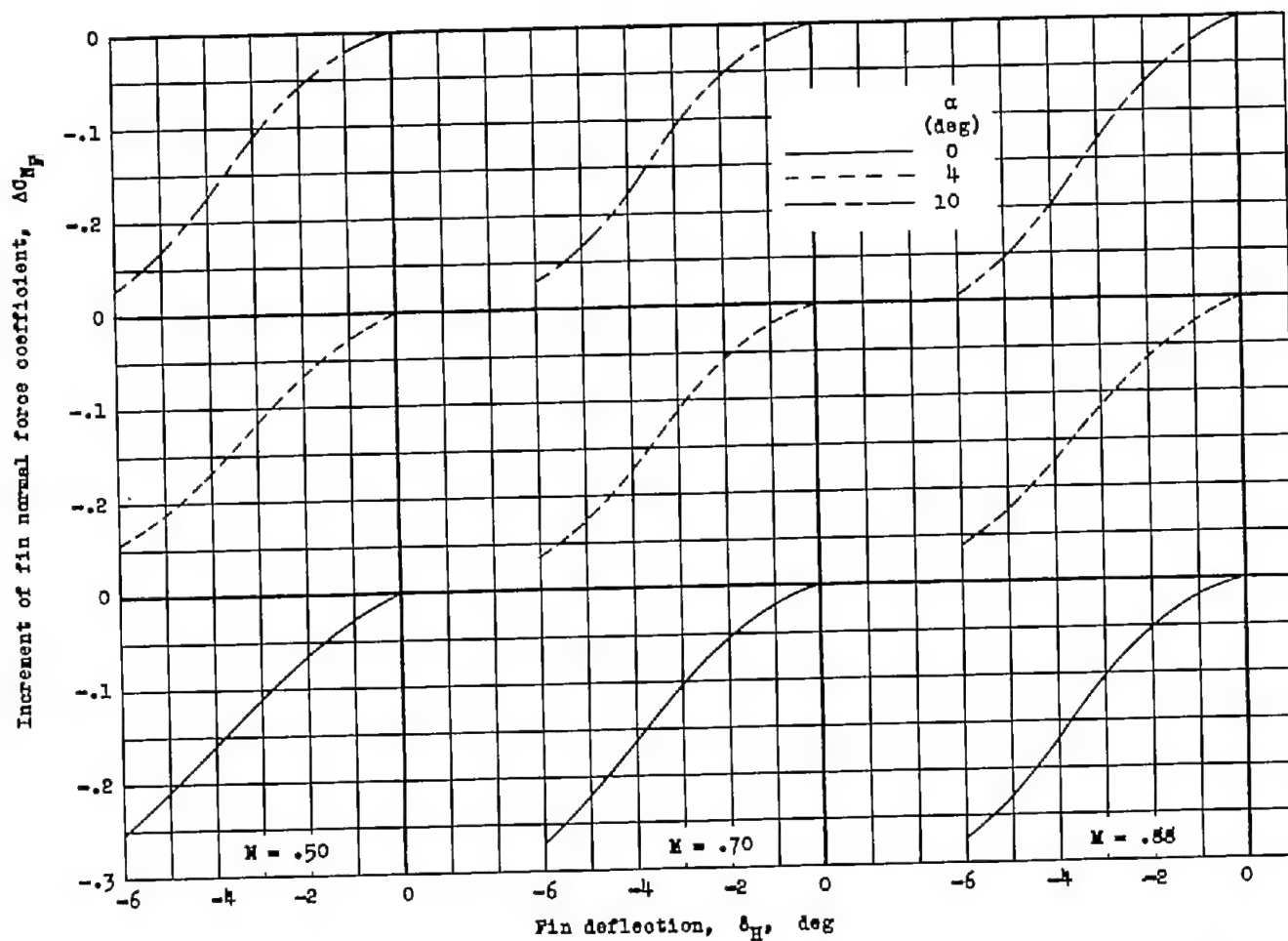
CONFIDENTIAL



(a) Variation of fin normal-force coefficient with angle of attack for four pitch-deflection angles.

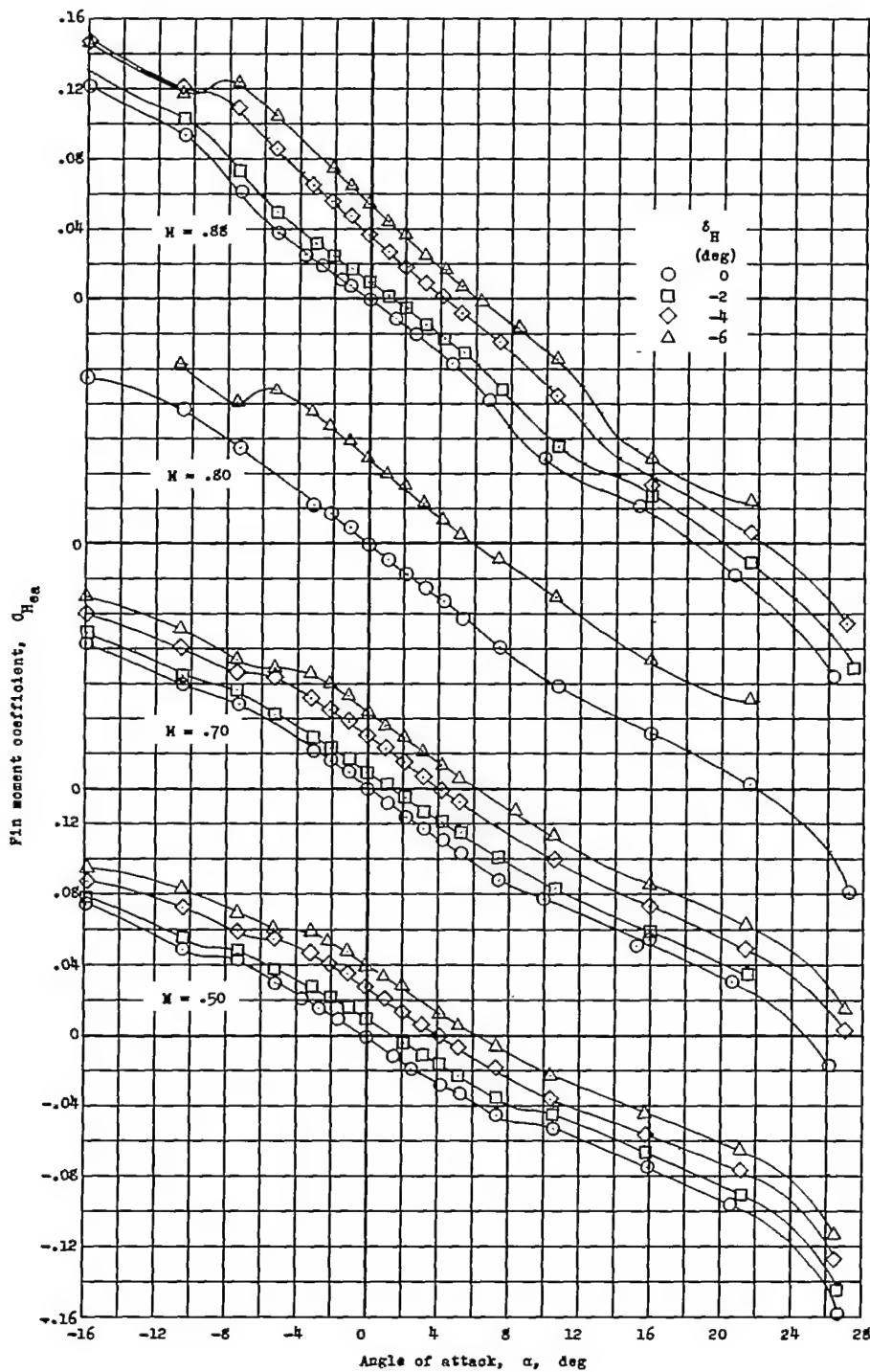
Figure 9.- Horizontal-fin normal-force coefficients for a wingless fin-controlled missile model at four Mach numbers. $\beta = 0^\circ$; $\delta_V = 0^\circ$.

CONFIDENTIAL



(b) Incremental values of fin normal-force coefficient due to fin deflection for three angles of attack.

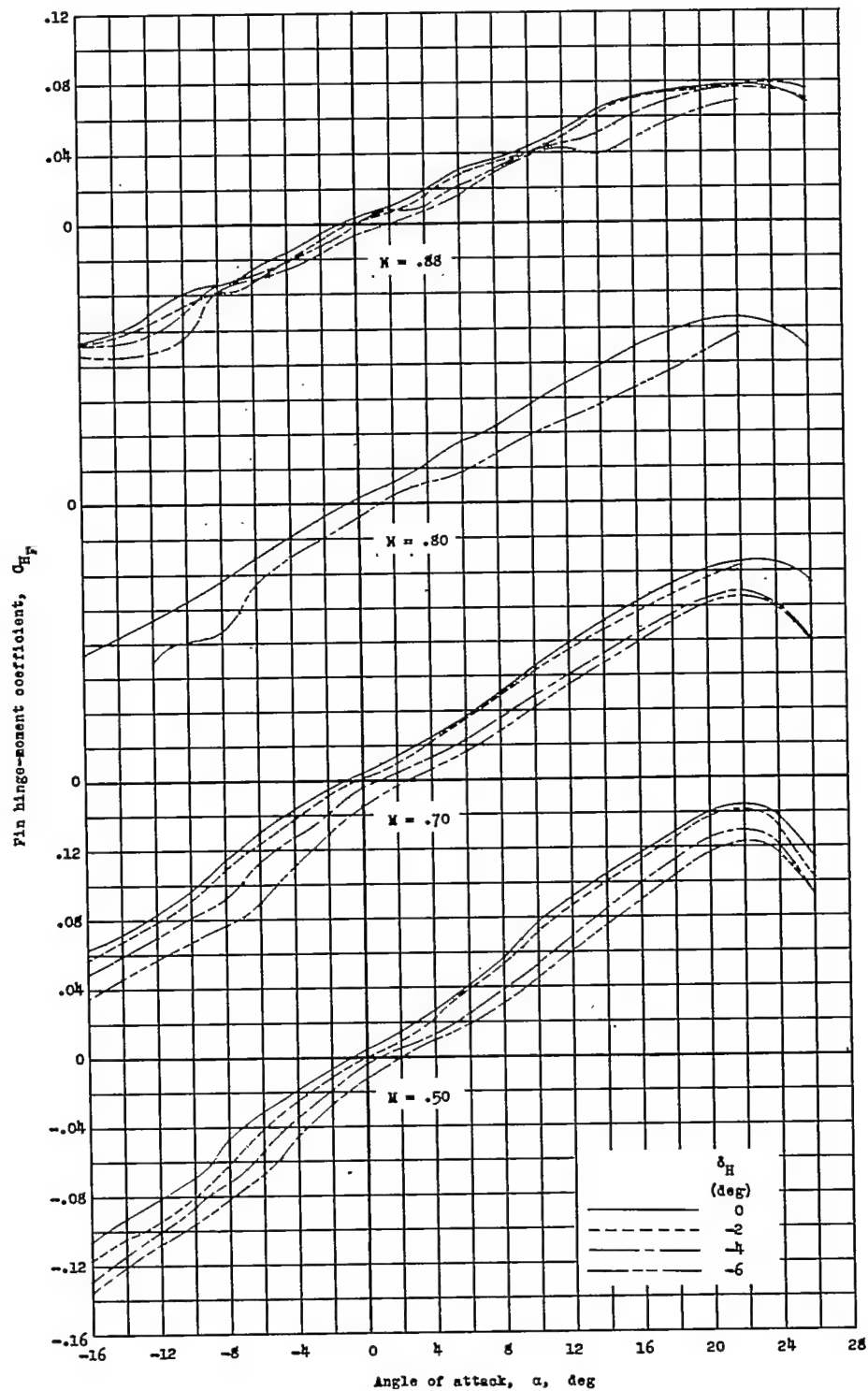
Figure 9.- Concluded.

~~CONFIDENTIAL~~

(a) Variation of fin moment coefficient (about electrical axis) with angle of attack for four pitch-deflection angles.

Figure 10.- Horizontal-fin moment coefficients for a wingless fin-controlled missile model at four Mach numbers.

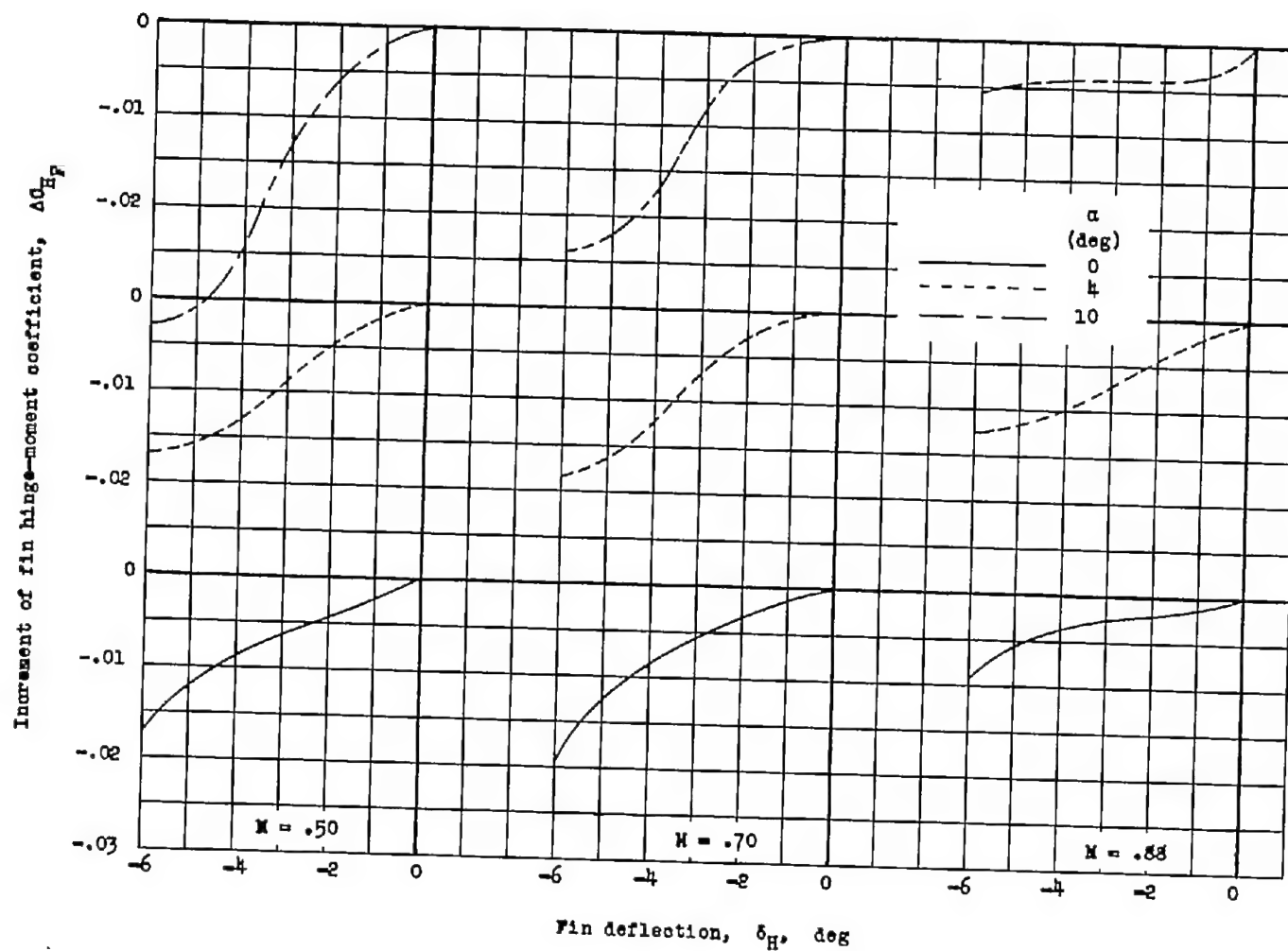
~~CONFIDENTIAL~~



(b) Variation of fin hinge-moment coefficient with angle of attack for four pitch deflection angles.

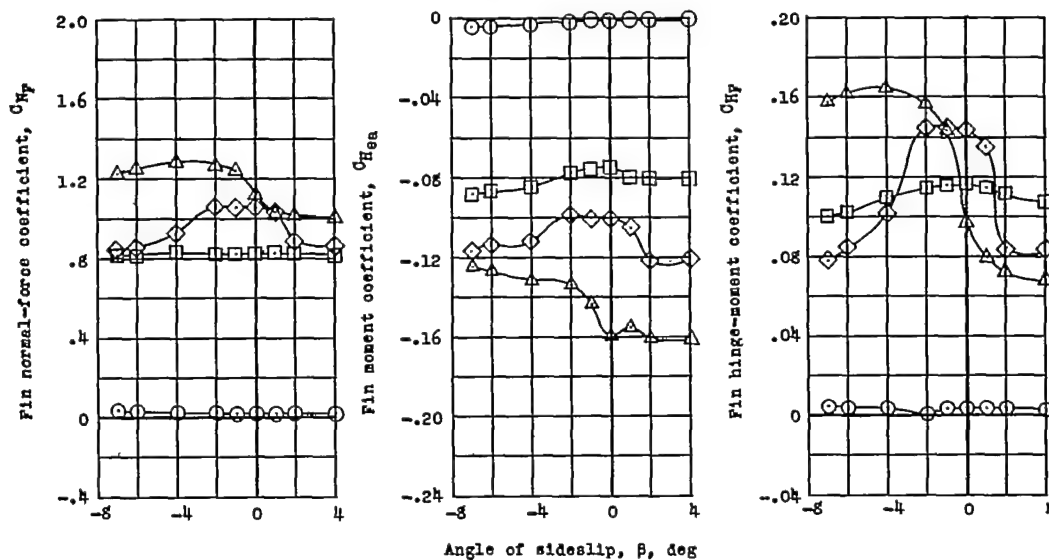
Figure 10.- Continued.

CONFIDENTIAL

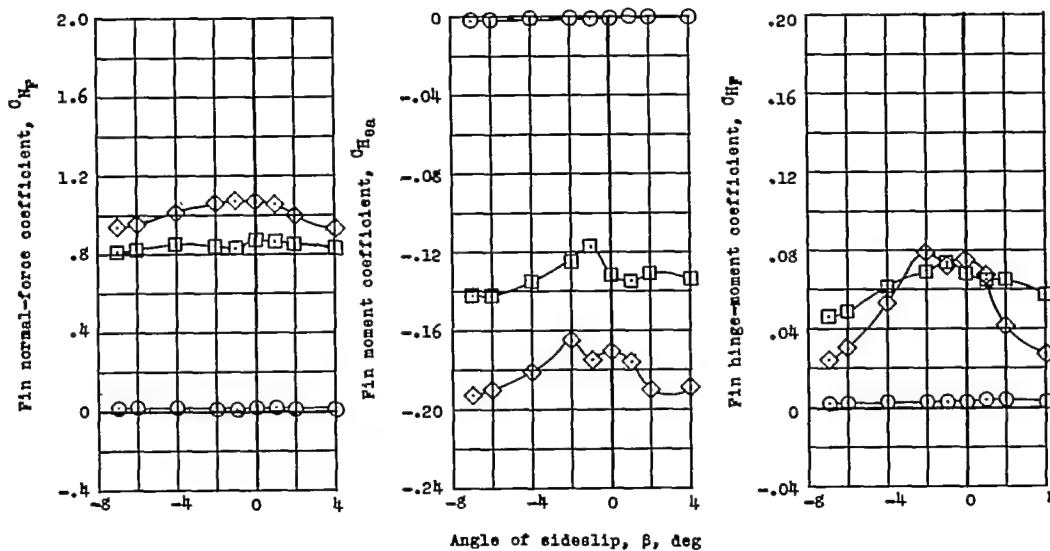


(c) Incremental values of fin hinge-moment coefficient due to fin deflection for three angles of attack.

Figure 10.- Concluded.



(a) $M = 0.50$.

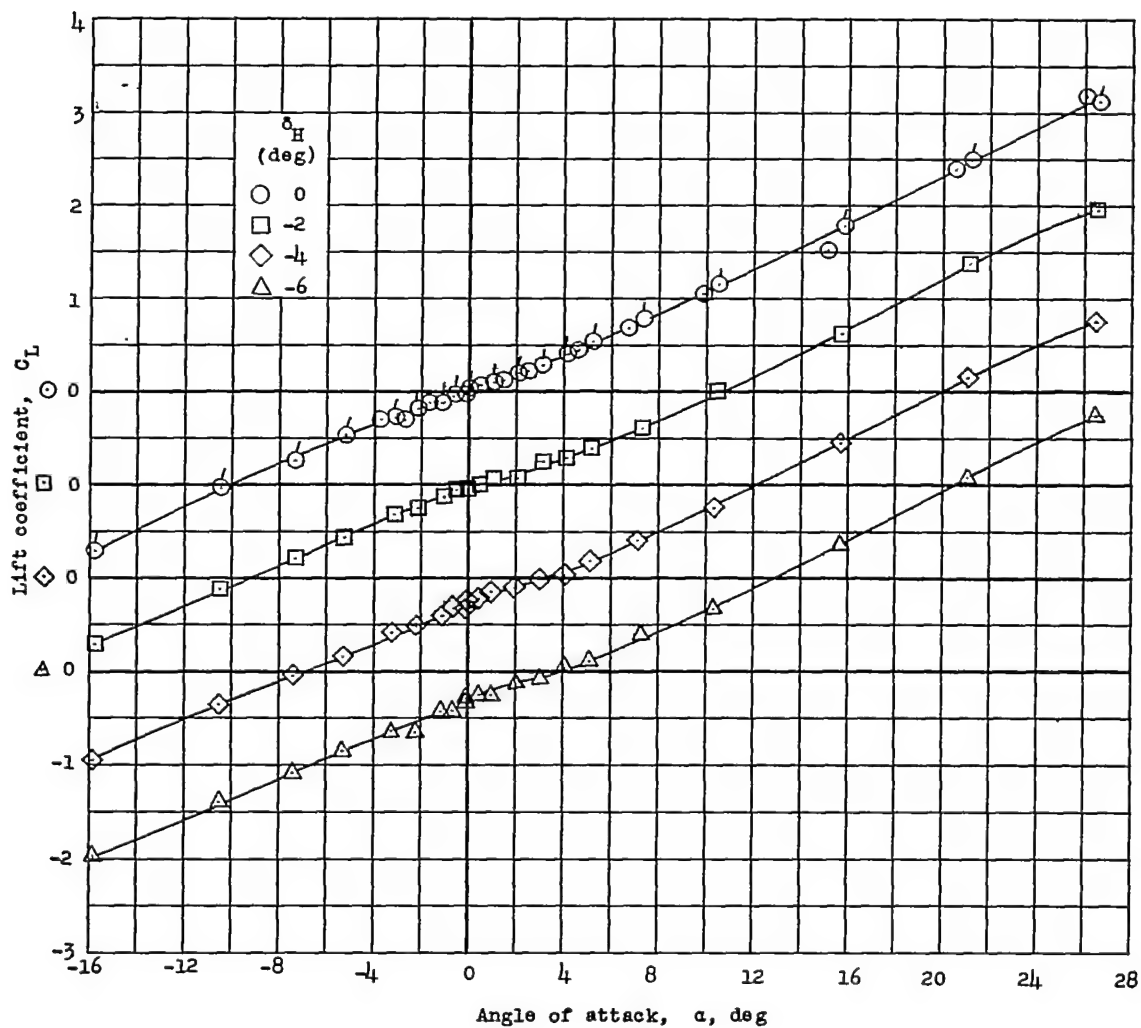


$M = .50$
 α , deg
 ○ 0
 □ 15.8
 ◇ 21.2
 △ 26.5

$M = .88$
 α , deg
 ○ 0
 □ 16.0
 ◇ 21.5

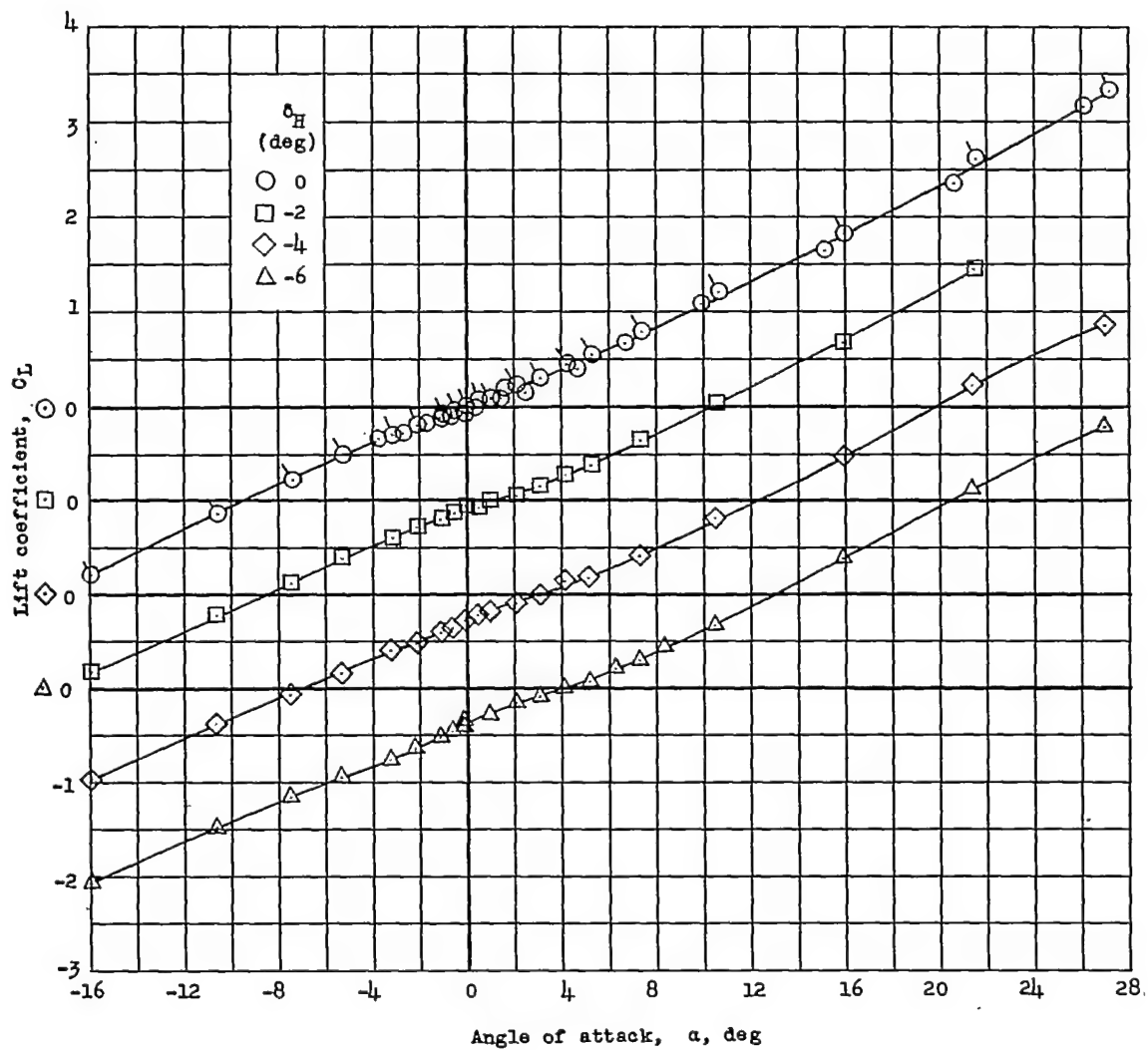
(b) $M = 0.88$.

Figure 11.- Variation of horizontal-fin normal-force and moment coefficients with angle of sideslip for a wingless fin-controlled missile model at four angles of attack and two Mach numbers. $\delta_H = 0^\circ$; $\delta_V = 0^\circ$.



(a) $M = 0.50$.

Figure 12.- Variation of lift coefficient with angle of attack for a wingless fin-controlled missile model with the horizontal fins at four pitch-deflection angles. $\beta = 0^\circ$; $\delta\gamma = 0^\circ$.



(b) $M = 0.70$.

Figure 12.- Continued.

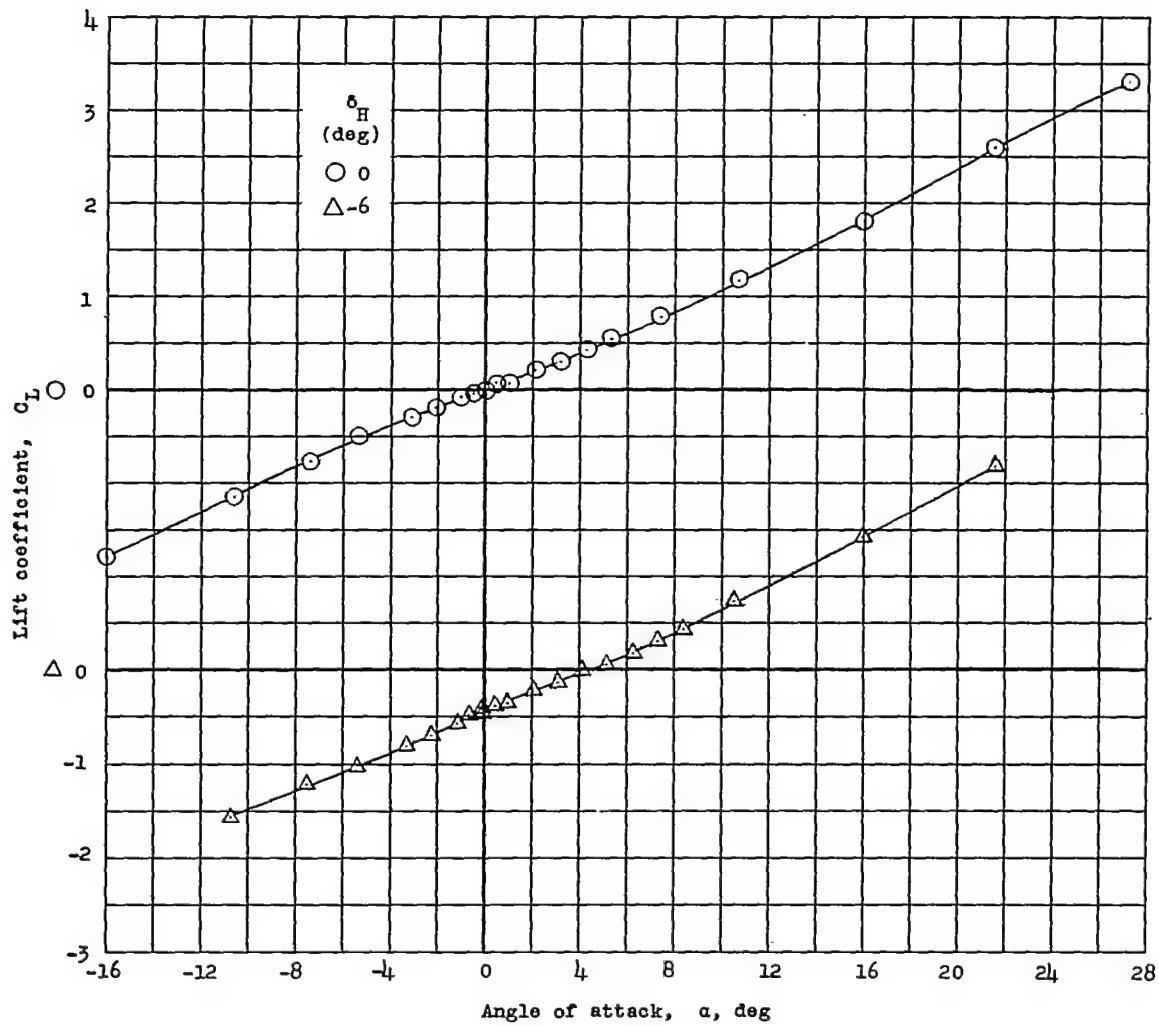
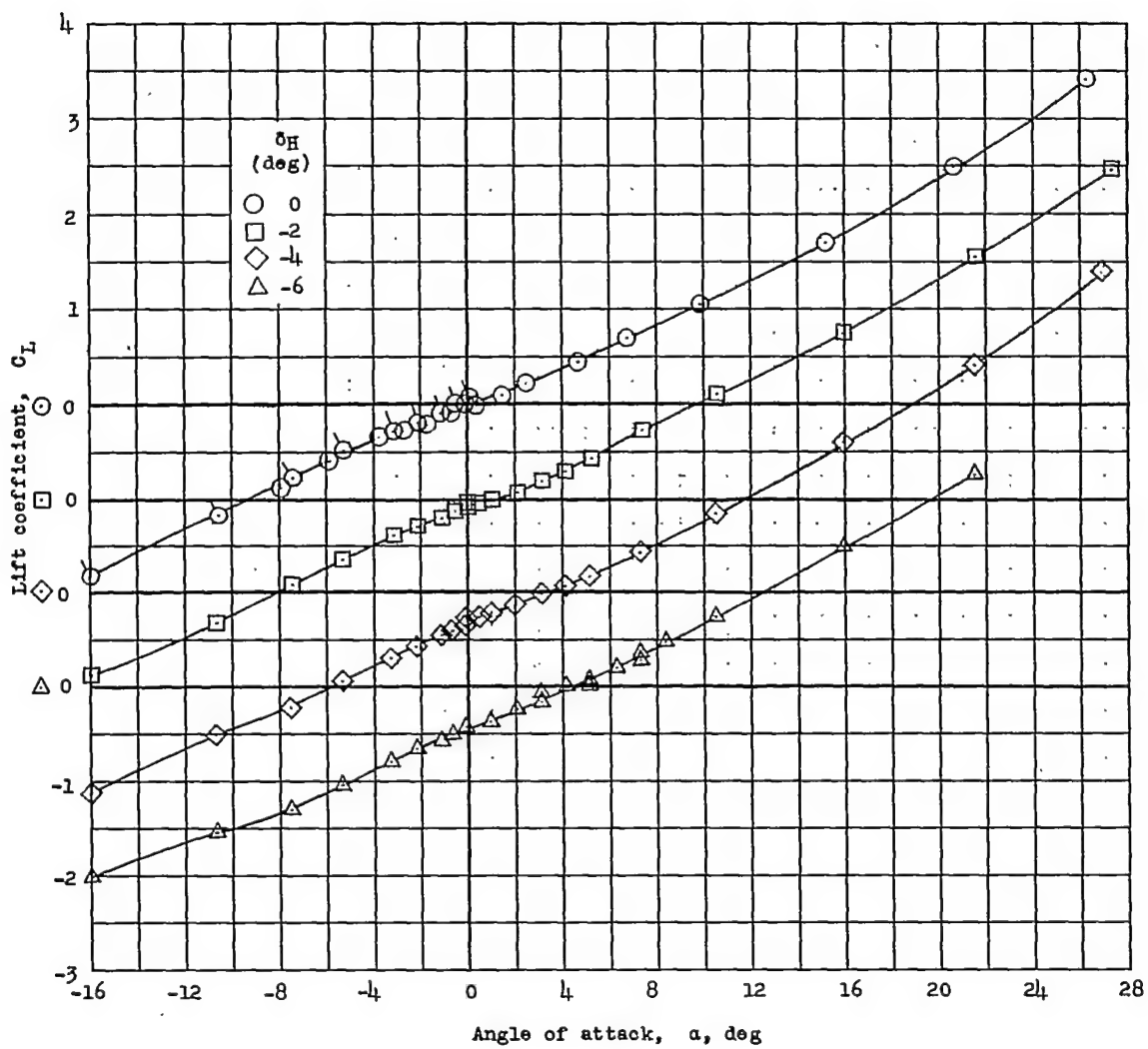
~~CONFIDENTIAL~~(c) $M = 0.80$.

Figure 12.- Continued.

~~CONFIDENTIAL~~



(d) $M = 0.88$.

Figure 12.- Concluded.

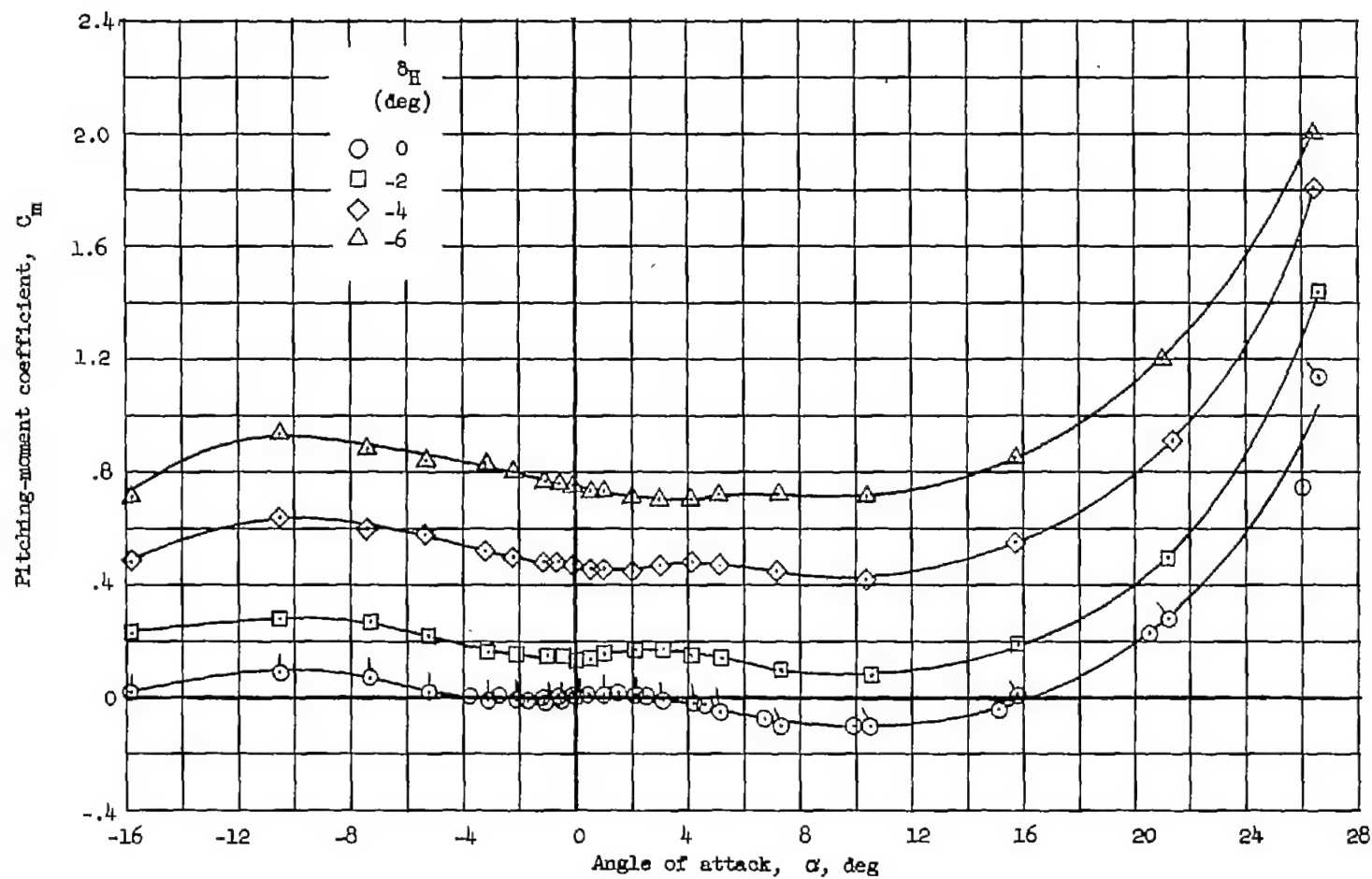
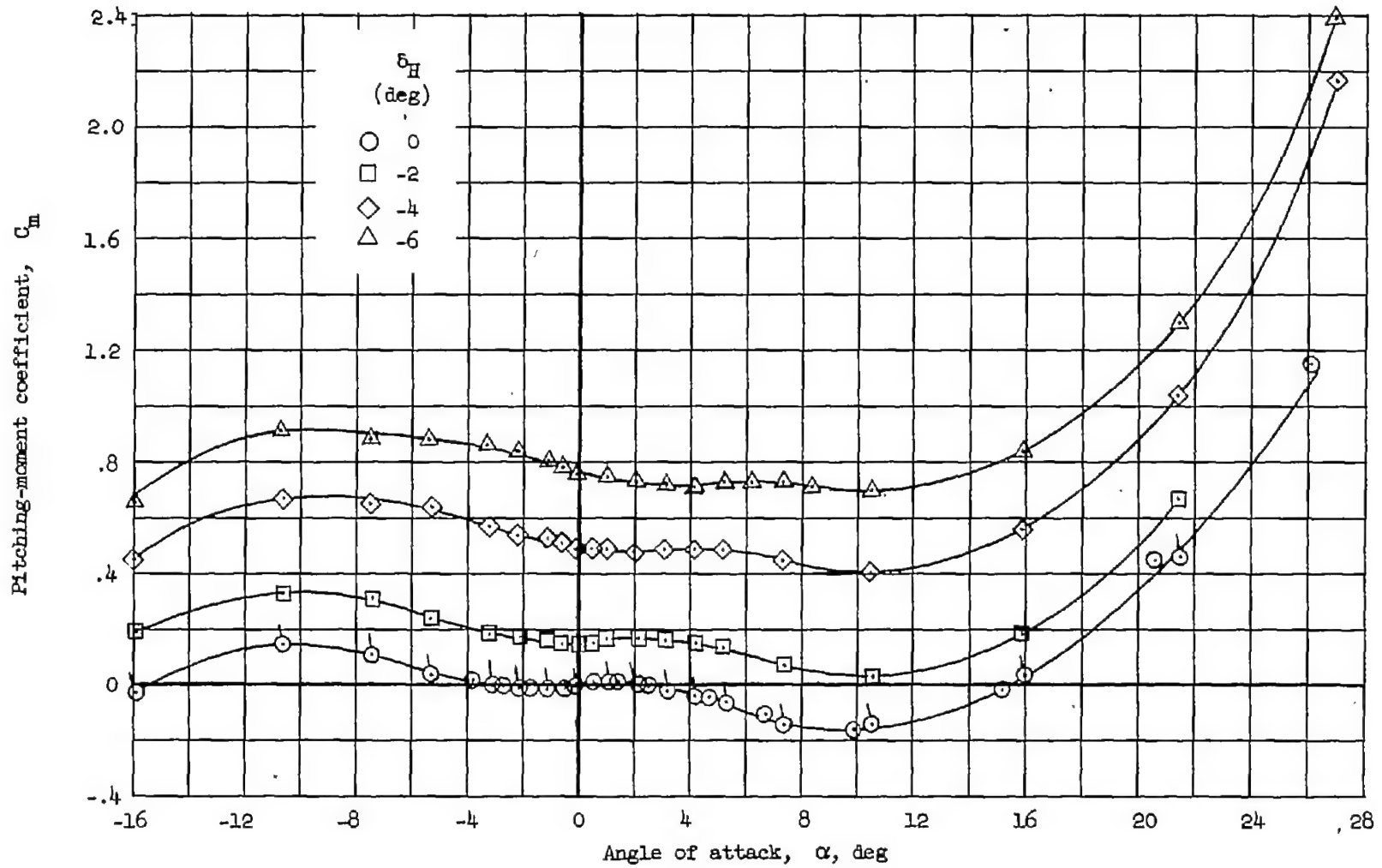
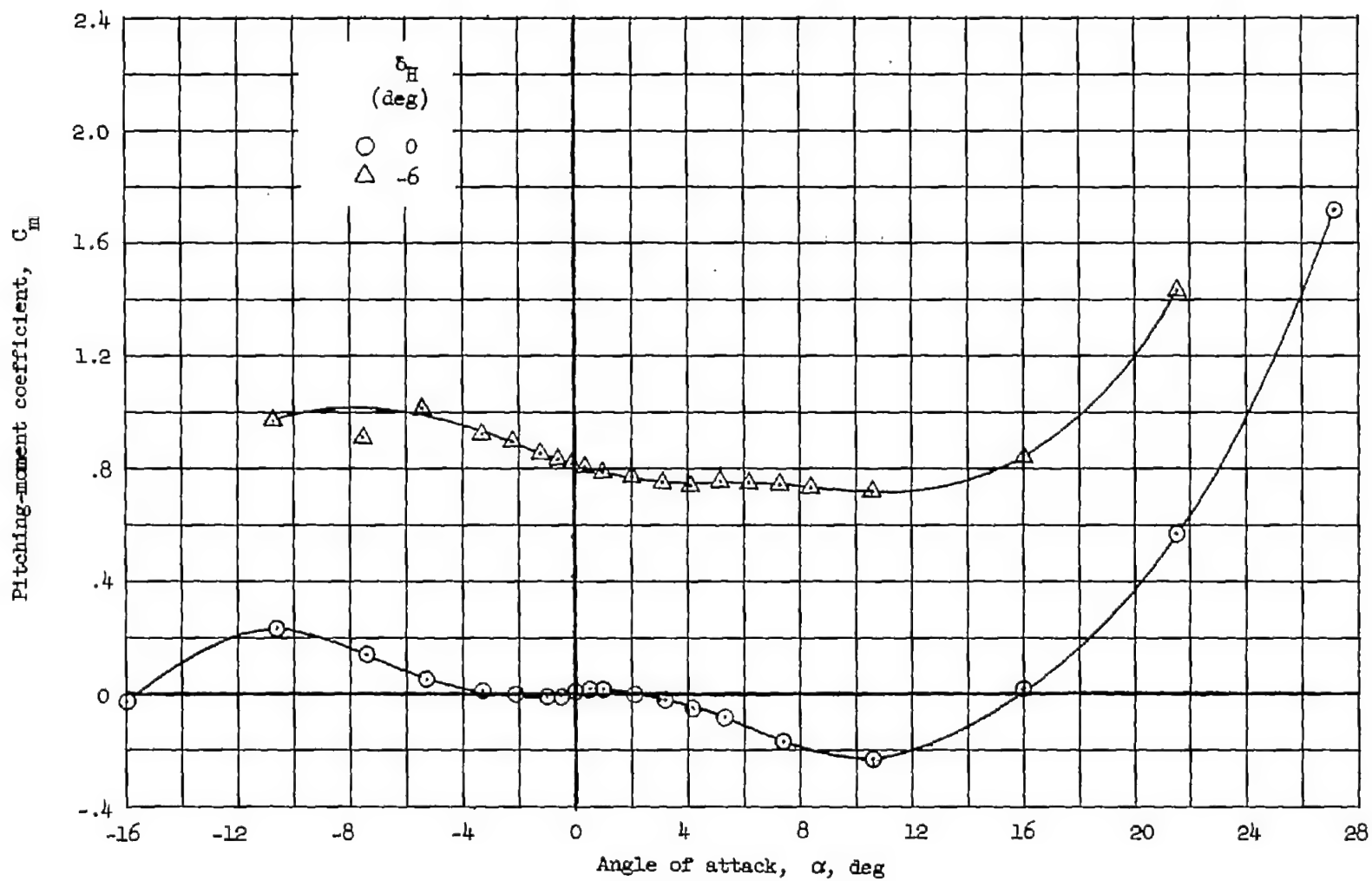
(a) $M = 0.50$.

Figure 13.- Variation of pitching-moment coefficient with angle of attack for a wingless fin-controlled missile model with the horizontal fins at four pitch-deflection angles. $\beta = 0^\circ$; $\delta_V = 0^\circ$.



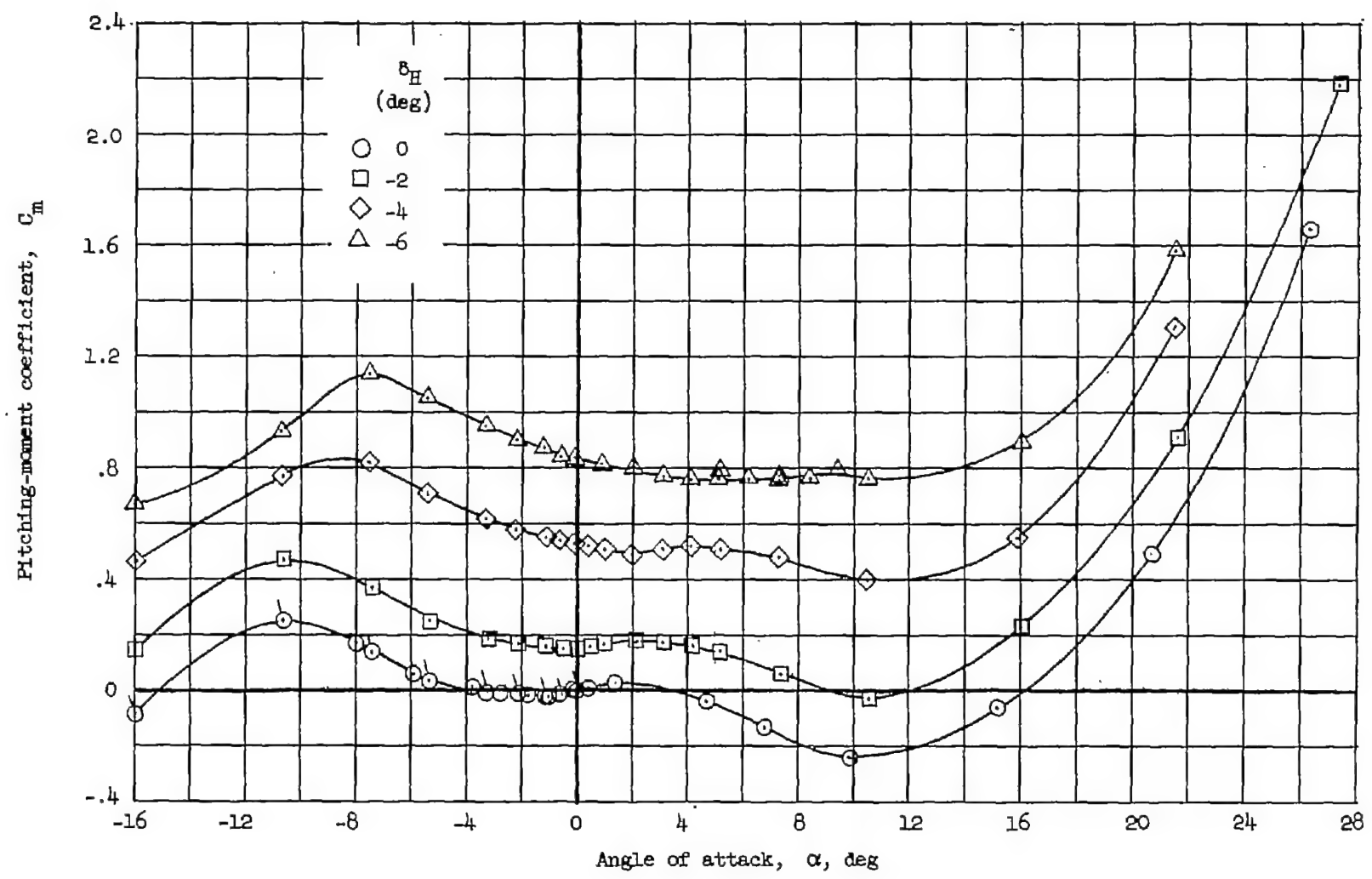
(b) $M = 0.70$.

Figure 13.- Continued.



(c) $M = 0.80$.

Figure 13.- Continued.



(d) $M = 0.88$.

Figure 13.- Concluded.

CONFIDENTIAL

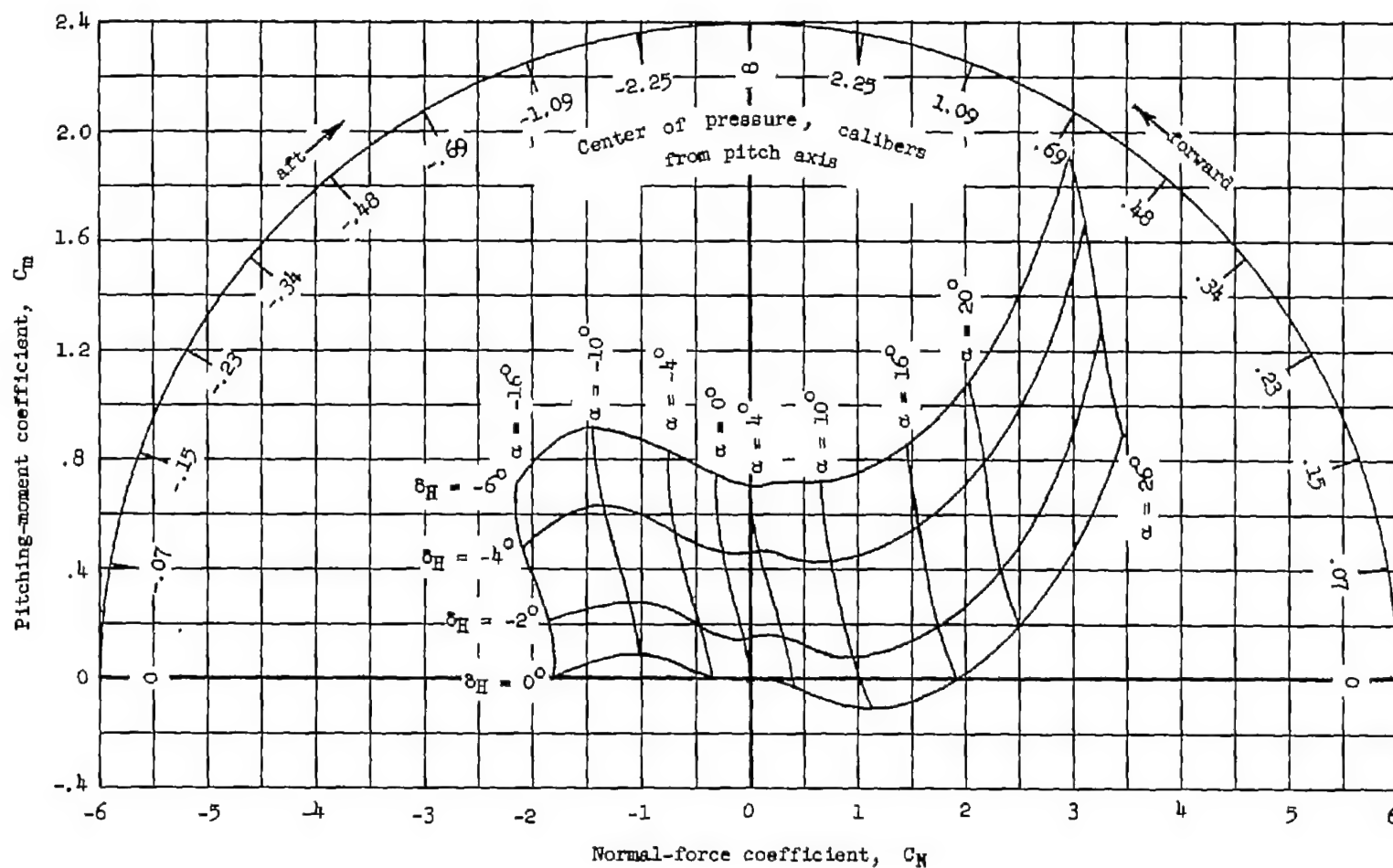
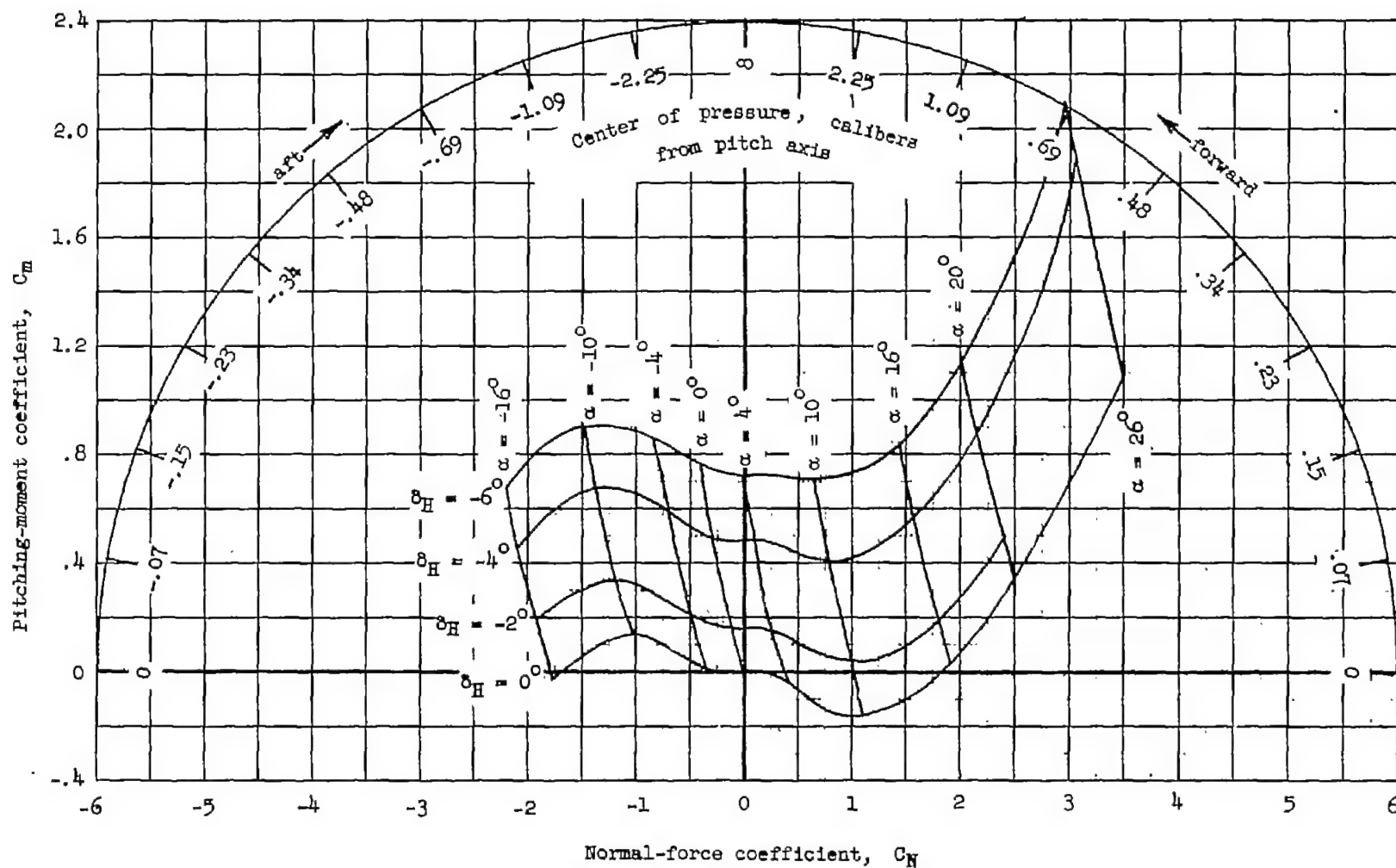
(a) $M = 0.50$.

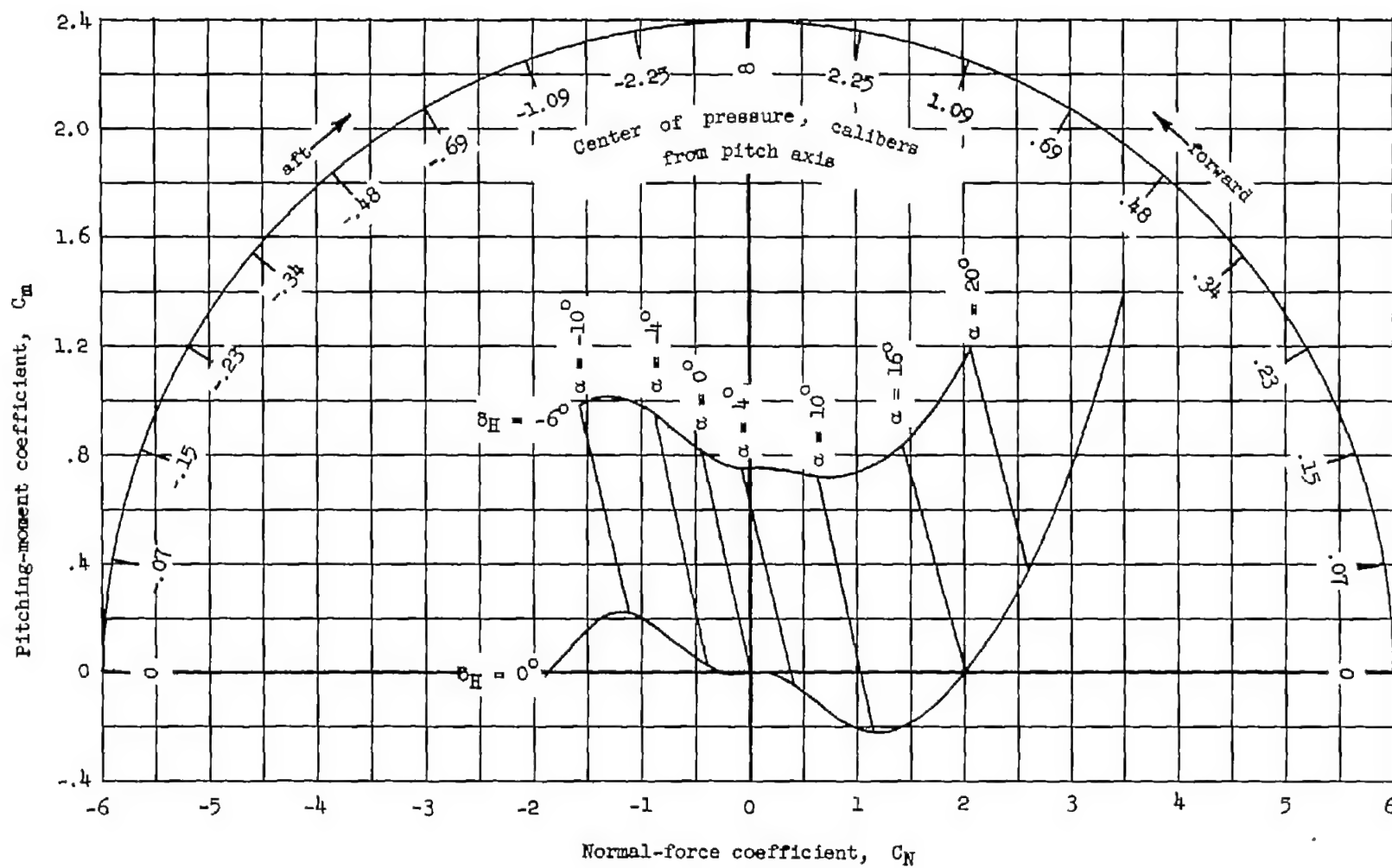
Figure 14.- Variation of pitching-moment coefficient with normal-force coefficient for a wingless fin-controlled missile model at several angles of attack and with the horizontal fins at four pitch-deflection angles. $\beta = 0^\circ$; $\delta_V = 0^\circ$.

CONFIDENTIAL



(b) $M = 0.70$.

Figure 14.- Continued.



(c) $M = 0.80$.

Figure 14.- Continued.

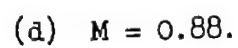


Figure 14.- Concluded.

CONFIDENTIAL

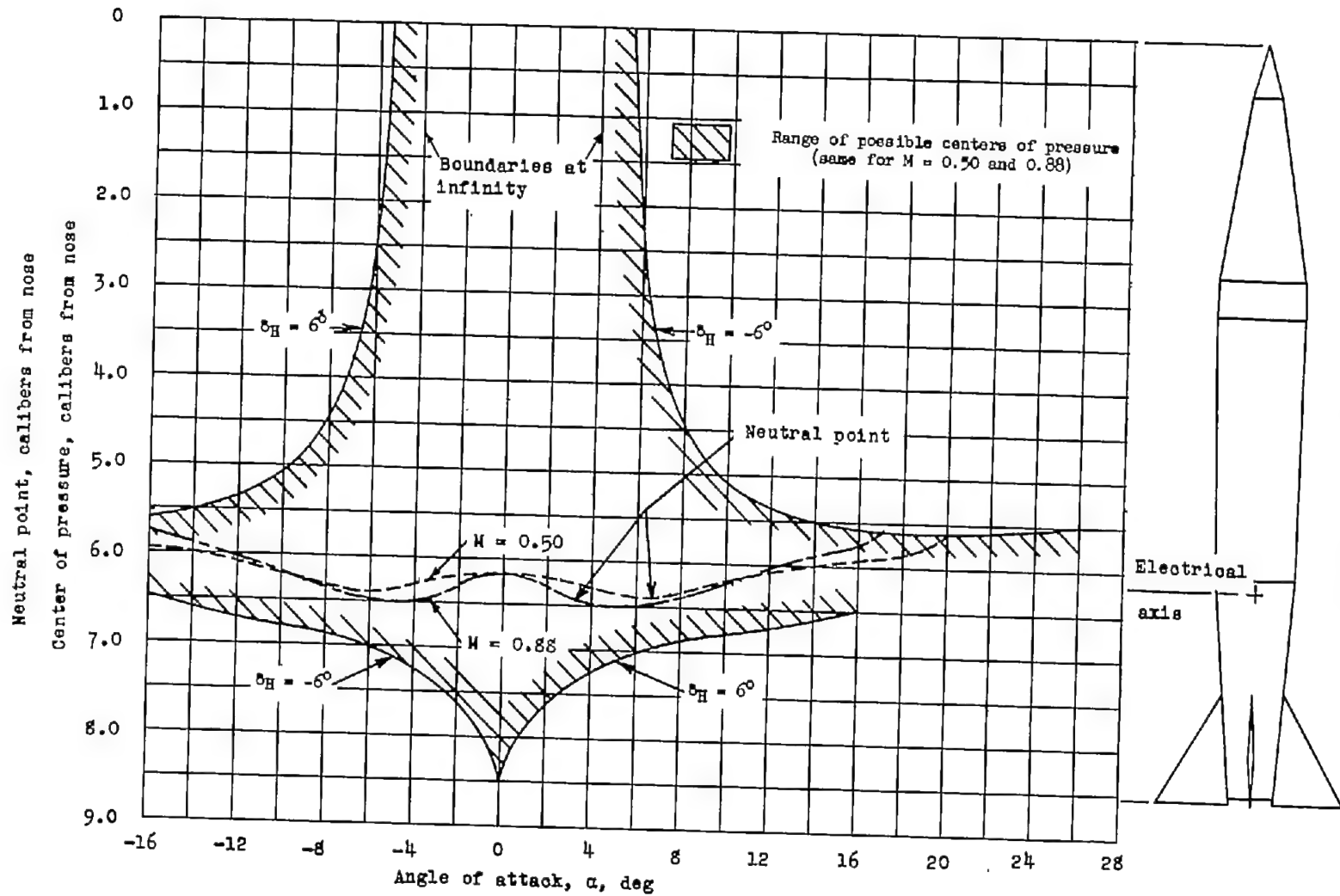
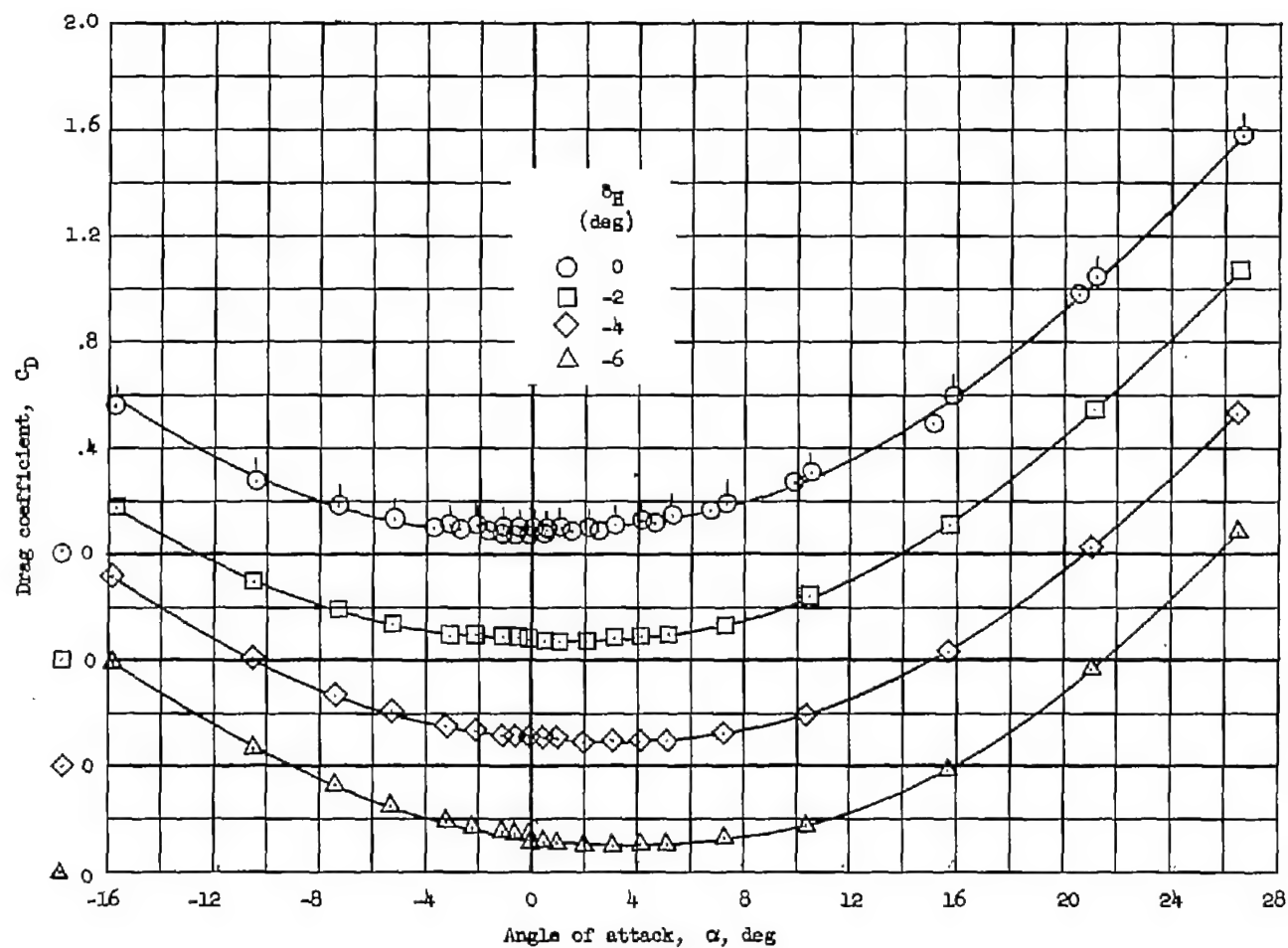


Figure 15.- Center-of-pressure positions for maximum pitch-deflection angles and neutral-point positions through an angle-of-attack range for a wingless fin-controlled missile. $\beta = 0^\circ$.



(a) $M = 0.50$.

Figure 16.- Variation of drag coefficient with angle of attack for a wingless fin-controlled missile model with the horizontal fins at four pitch-deflection angles. $\beta = 0^\circ$; $\delta_V = 0^\circ$.

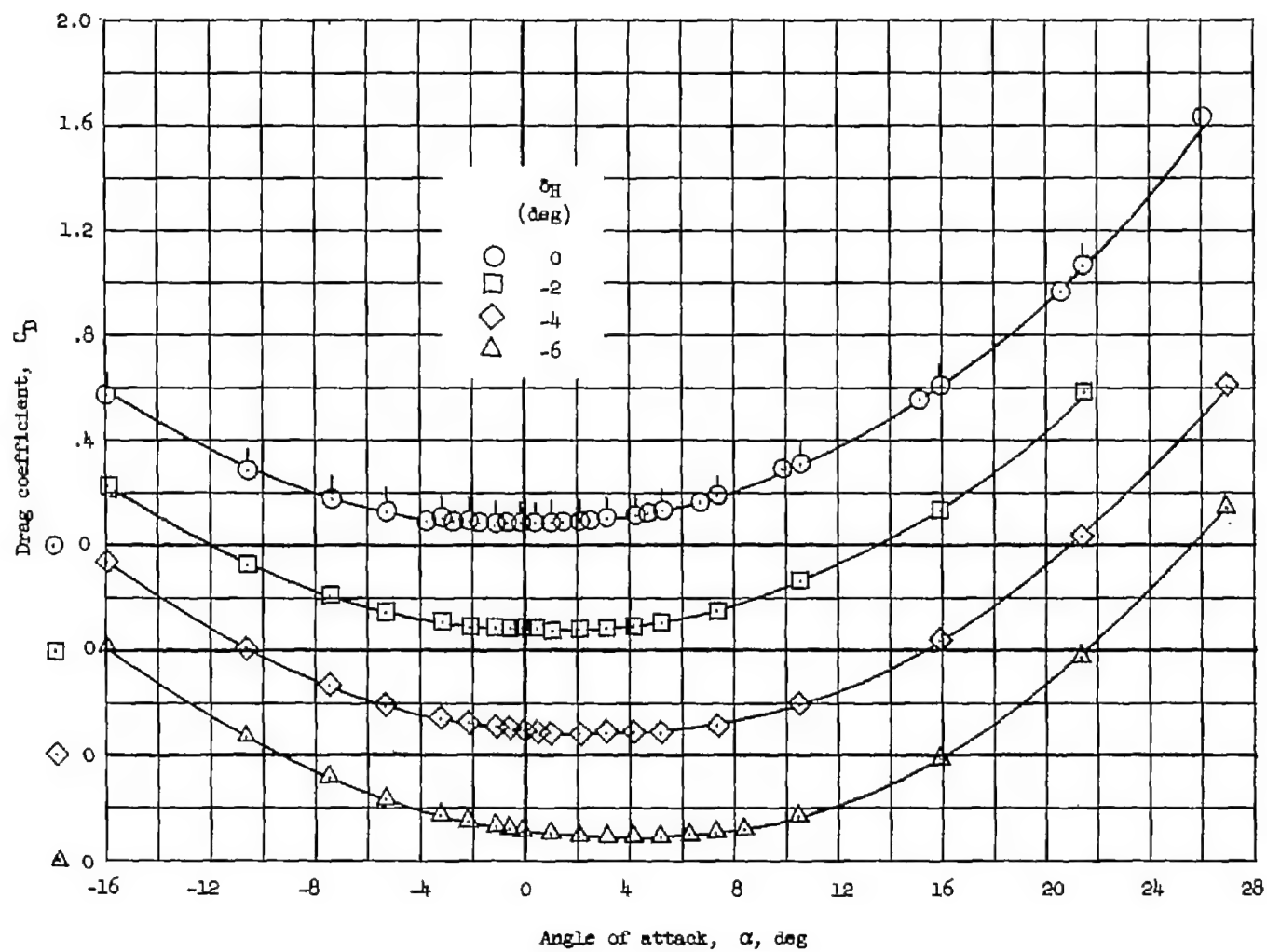
(b) $M = 0.70$.

Figure 16.- Continued.

CONFIDENTIAL

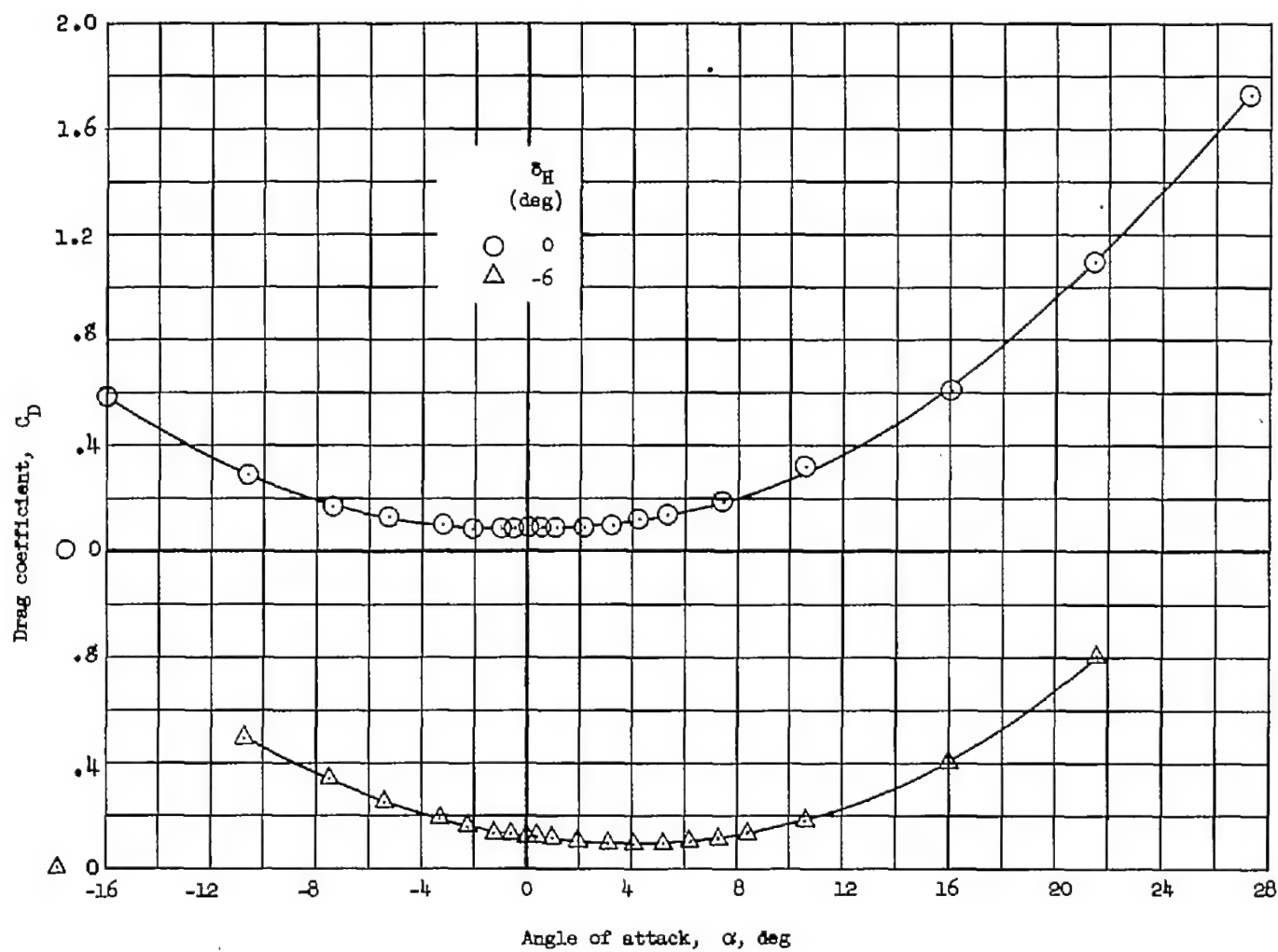
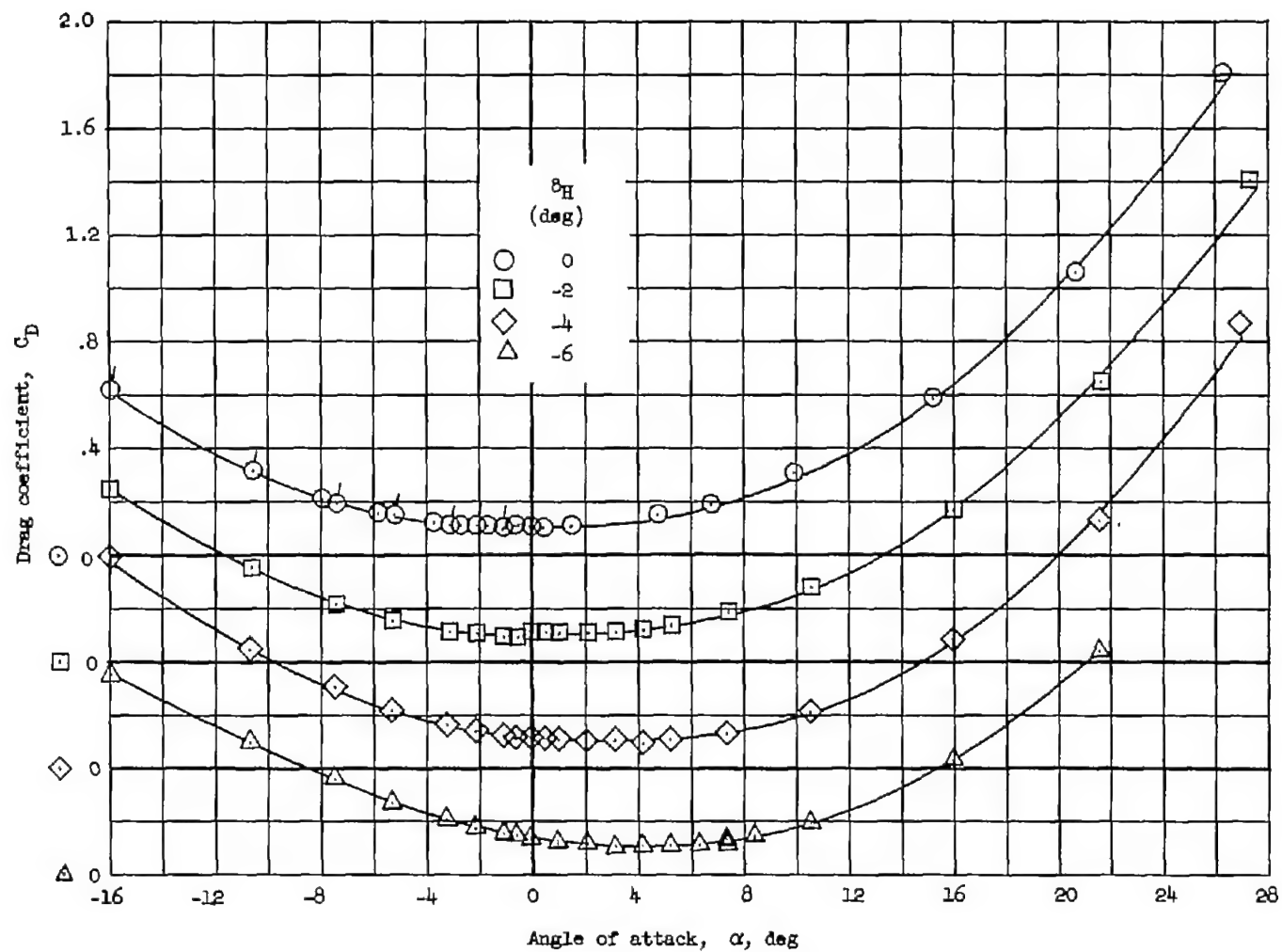
(c) $M = 0.80$.

Figure 16.- Continued.

CONFIDENTIAL

CONFIDENTIAL



(d) $M = 0.88$.

Figure 16.- Concluded.

CONFIDENTIAL

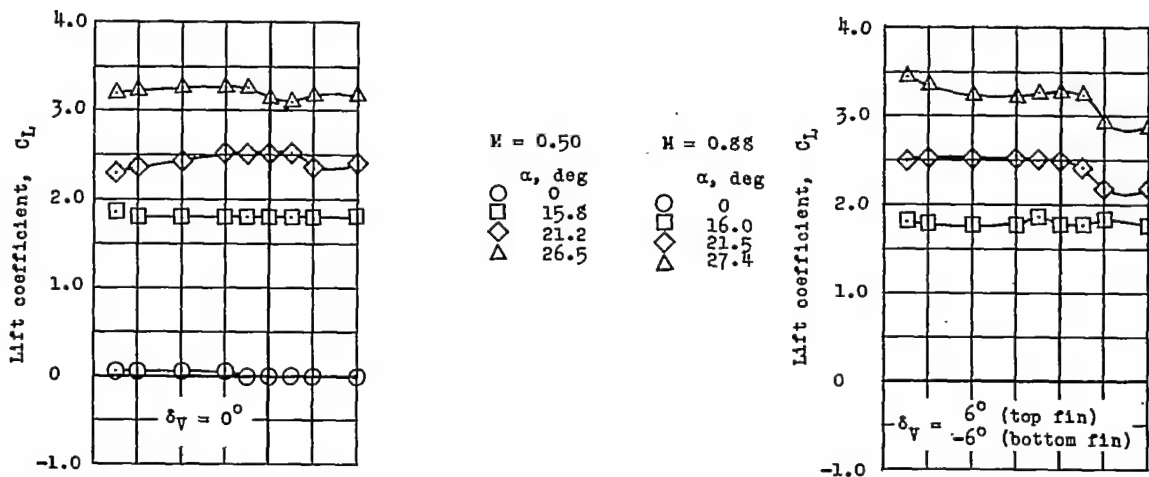
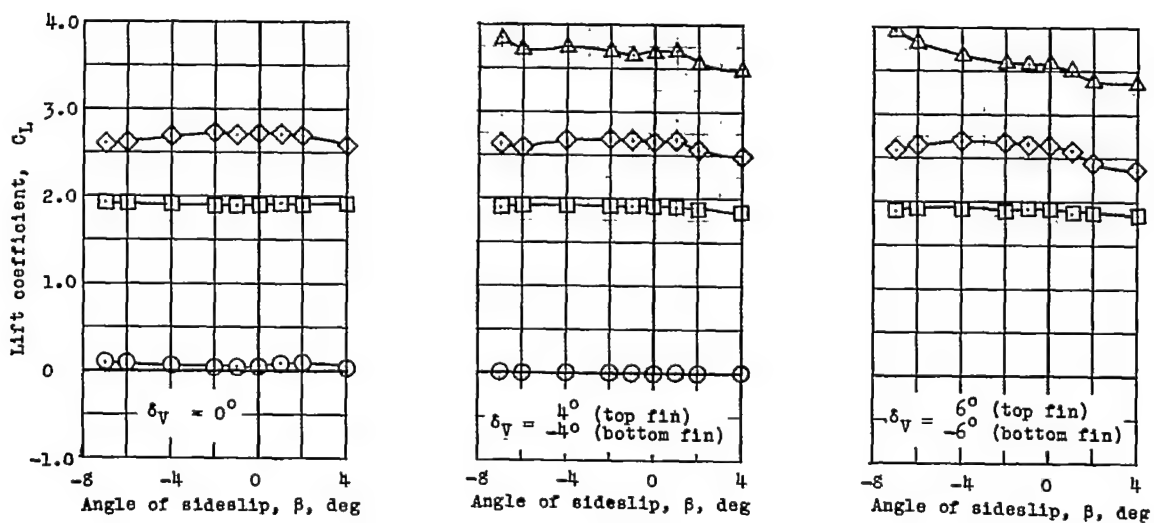
~~CONFIDENTIAL~~(a) $M = 0.50$.(b) $M = 0.88$.

Figure 17.- Variation of lift coefficient with angle of sideslip for a wingless fin-controlled missile model at four angles of attack and with the vertical fins at three roll-deflection angles. $\delta_H = 0^\circ$.

~~CONFIDENTIAL~~

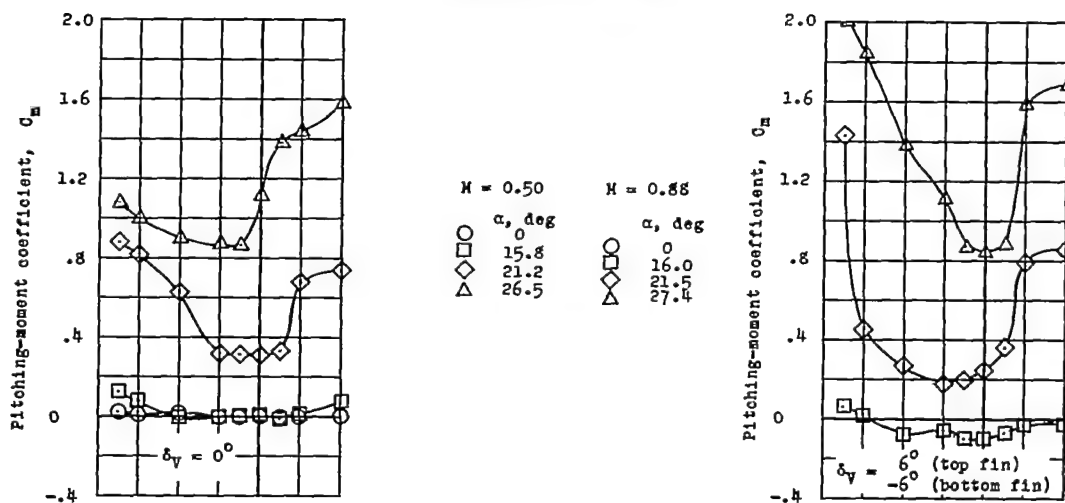
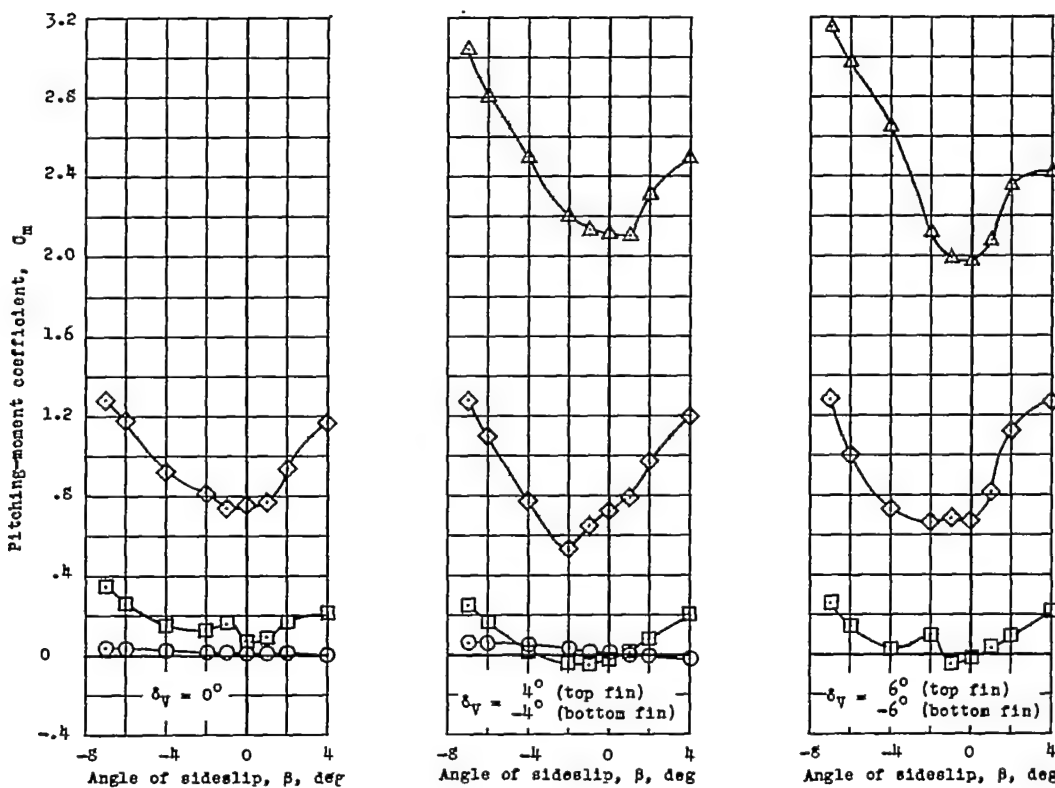
~~CONFIDENTIAL~~(a) $M = 0.50$.(b) $M = 0.88$.

Figure 18.- Variation of pitching-moment coefficient with angle of sideslip for a wingless fin-controlled missile model at four angles of attack and with the vertical fins at three roll-deflection angles. $\delta_H = 0^\circ$.

~~CONFIDENTIAL~~

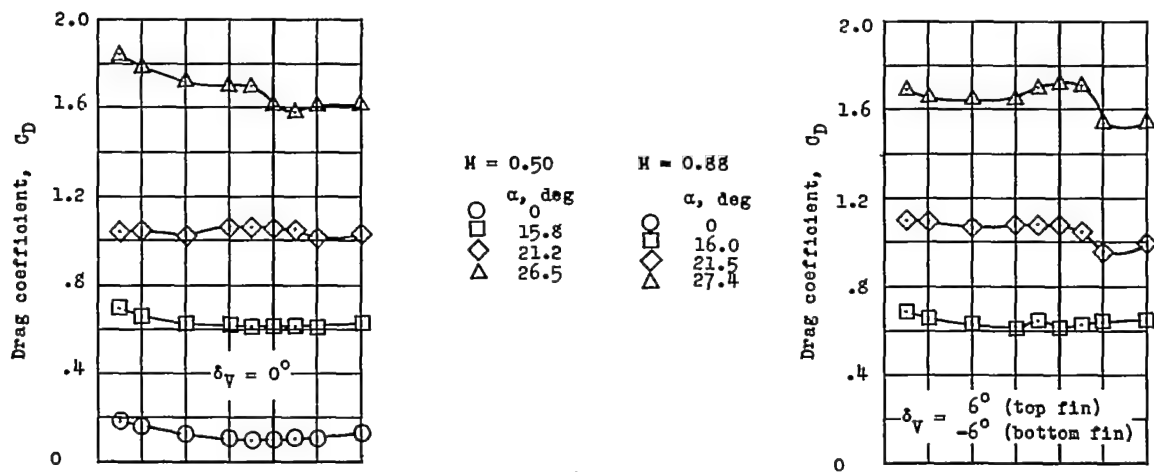
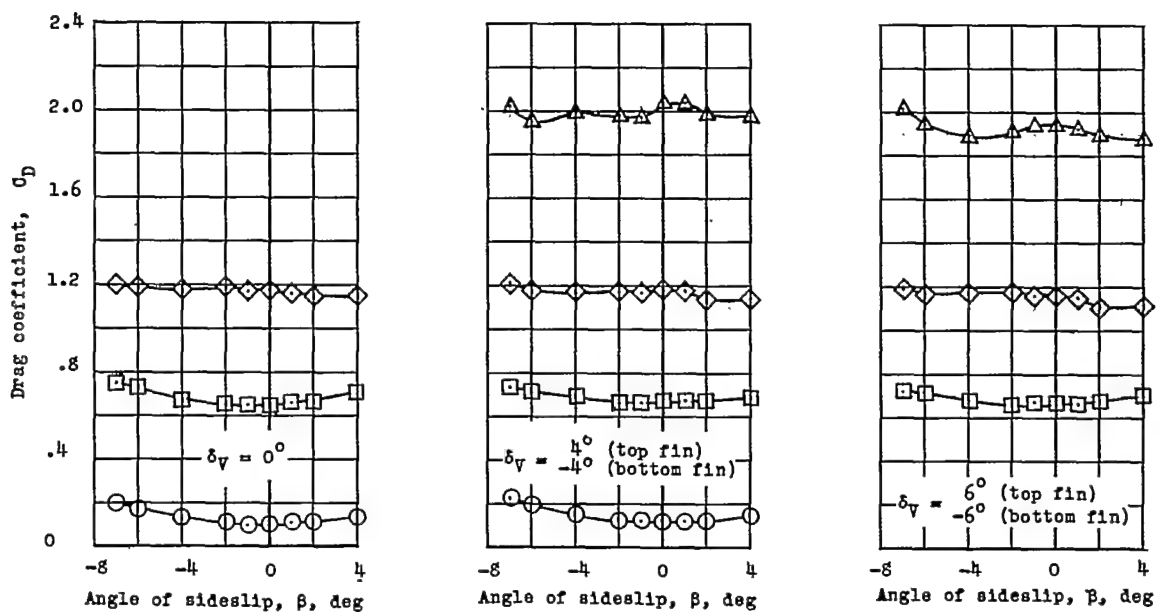
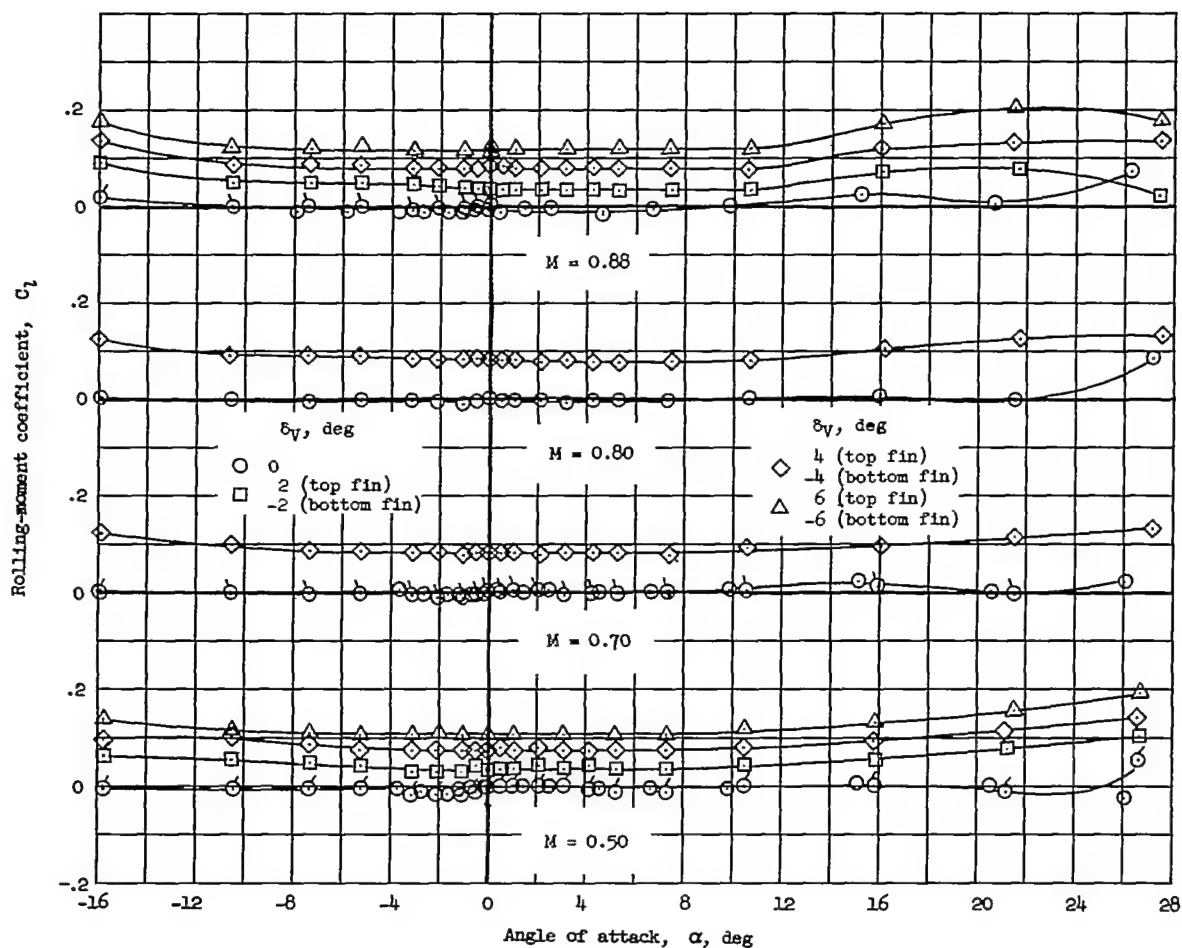
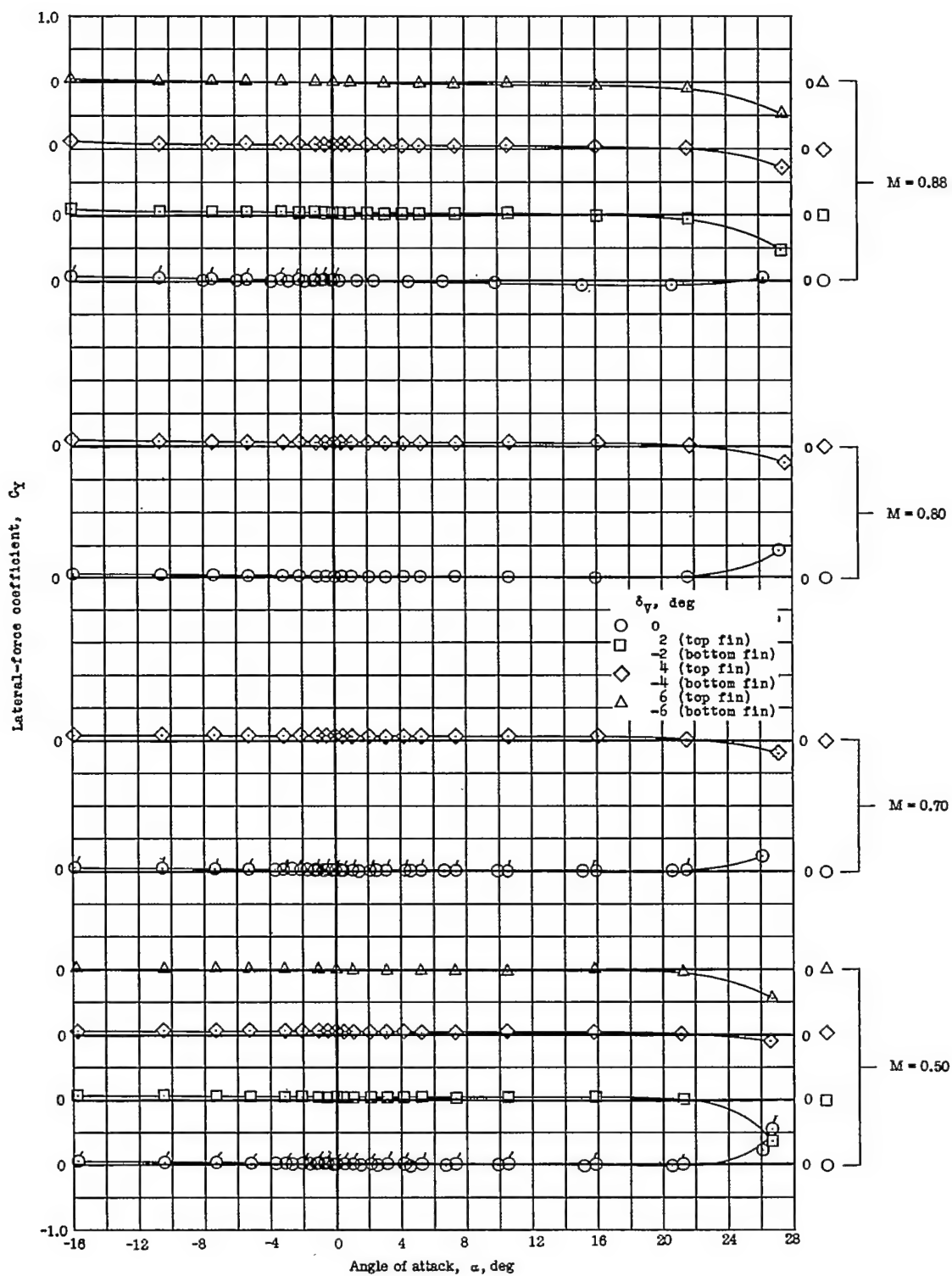
(a) $M = 0.50$.(b) $M = 0.88$.

Figure 19.- Variation of drag coefficient with angle of sideslip for a wingless fin-controlled missile model at four angles of attack and with the vertical fins at three roll-deflection angles. $\delta_H = 0^\circ$.



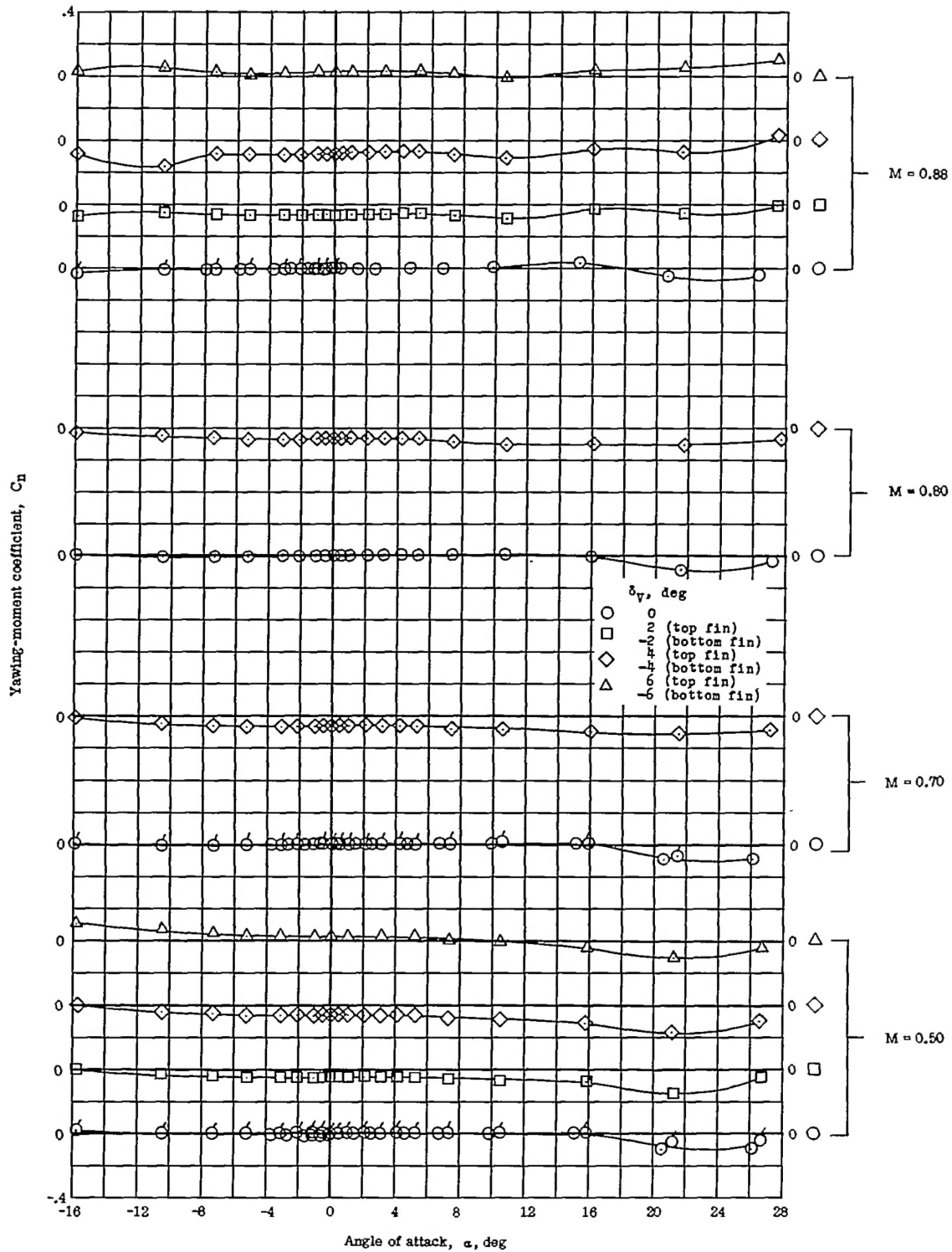
(a) Rolling moment.

Figure 20.-- Variation of lateral-force and moment coefficients with angle of attack for a wingless fin-controlled missile model at four Mach numbers and with the vertical fins set at four roll-deflection angles. $\beta = 0^\circ$; $\delta_H = 0^\circ$.



(b) Lateral force.

Figure 20.- Continued.

~~CONFIDENTIAL~~

(c) Yawing moment.

Figure 20.- Concluded.

~~CONFIDENTIAL~~

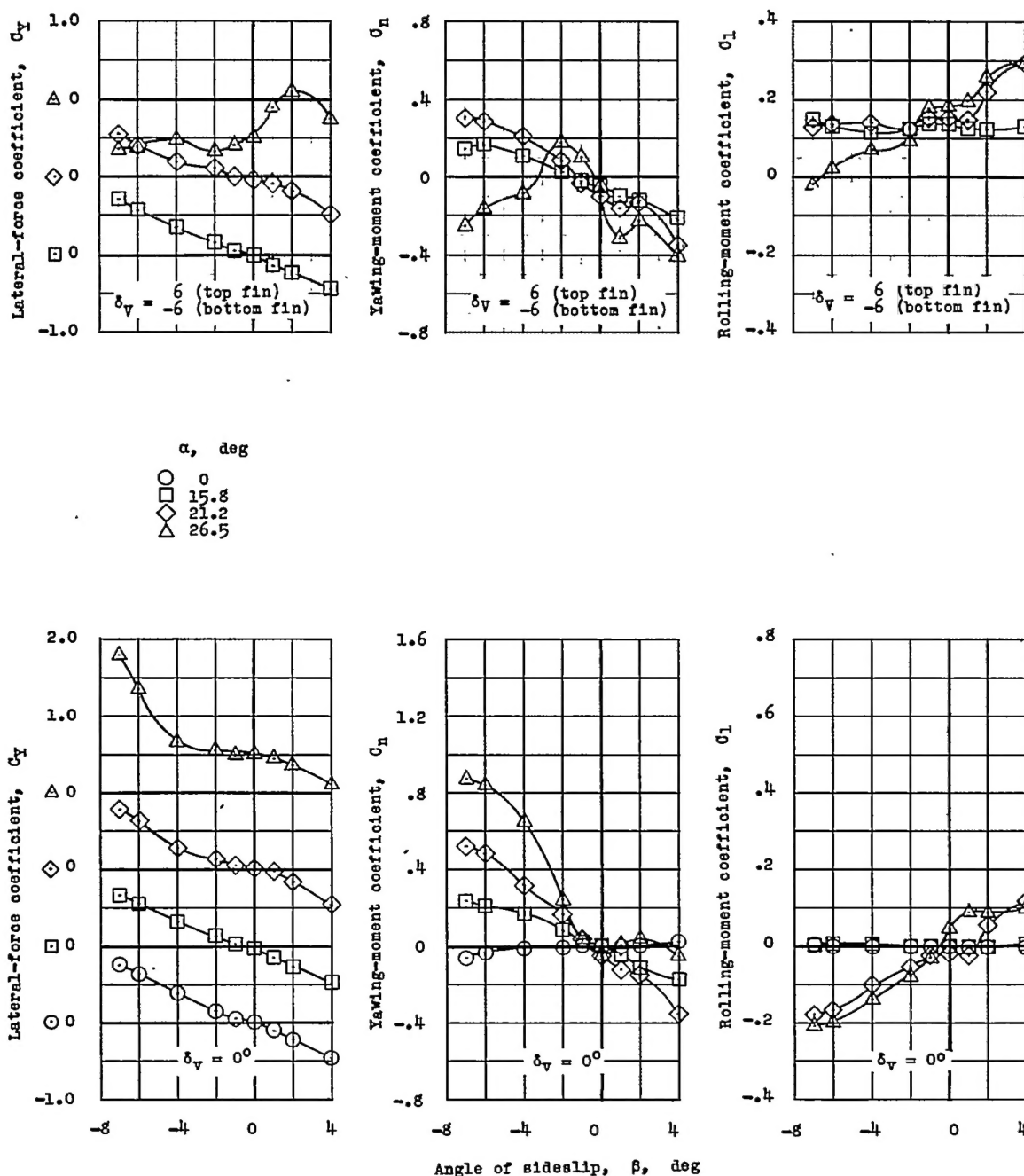
(a) $M = 0.50$.

Figure 21.- Variation of lateral-force and moment coefficients with angle of sideslip for a wingless fin-controlled missile model at four angles of attack and through a range of four Mach numbers. $\delta_H = 0^\circ$.

CONFIDENTIAL

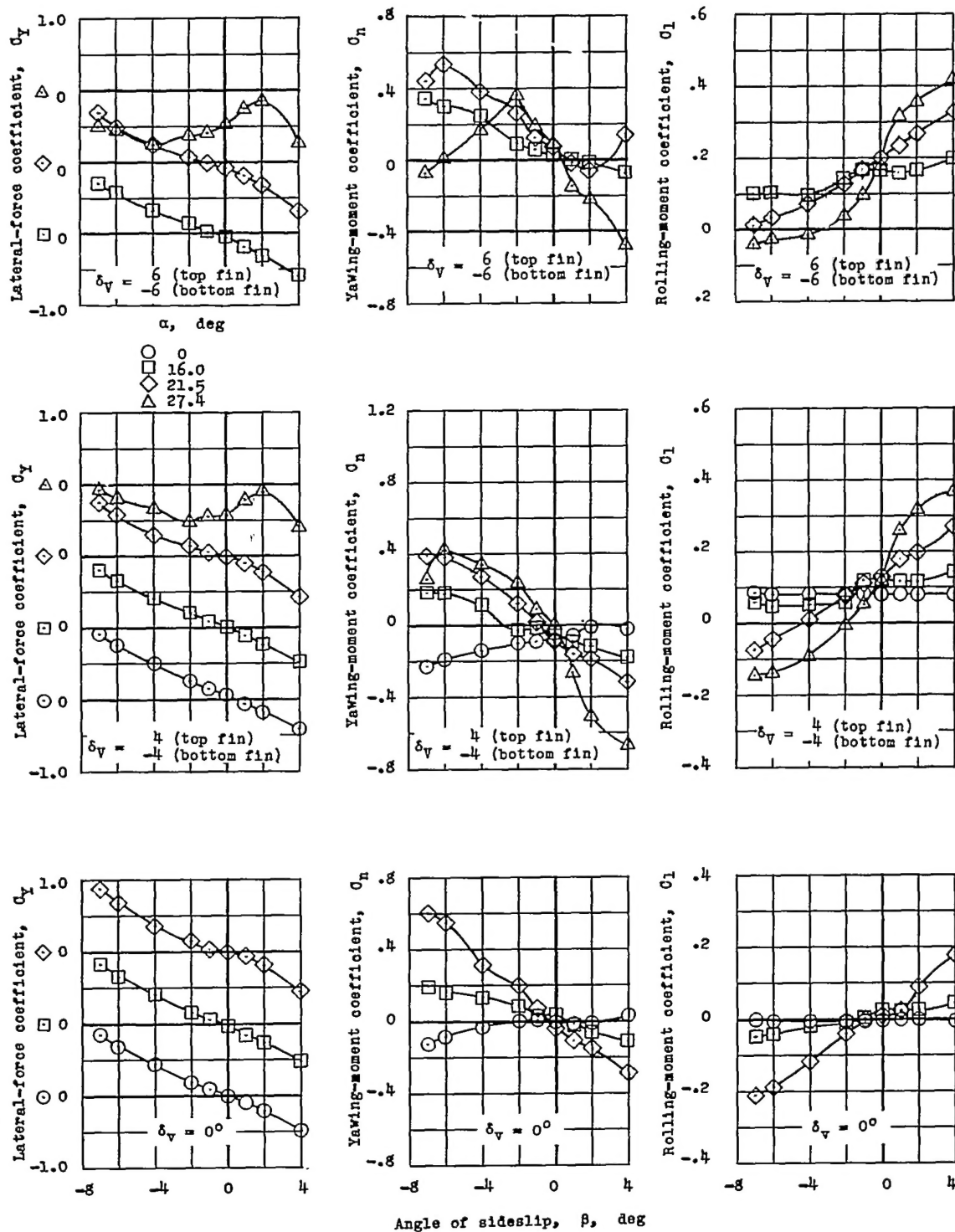
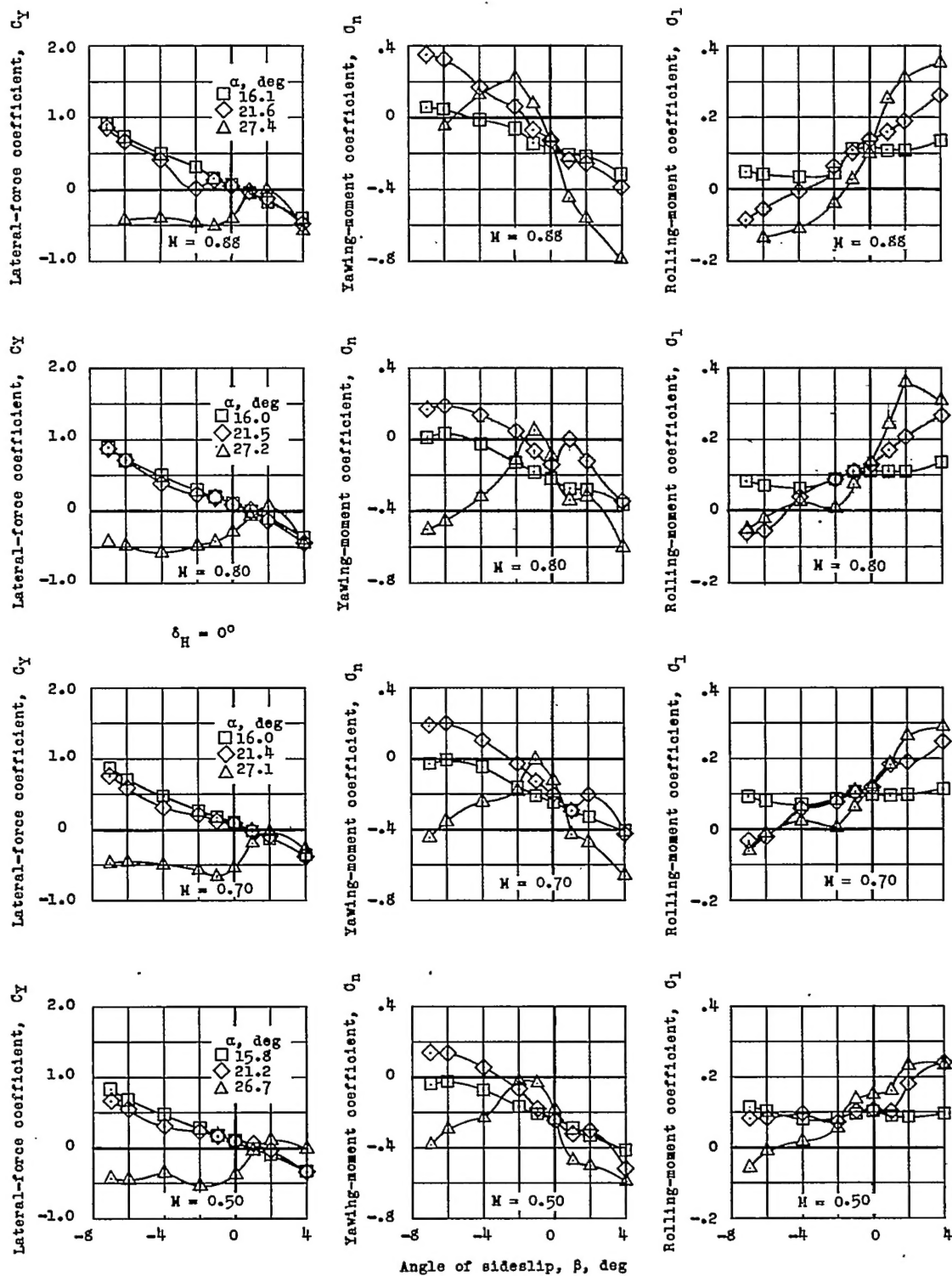
(b) $M = 0.88$.

Figure 21.- Continued.

CONFIDENTIAL



(c) $\delta_V = 6$ (top fin), $\delta_V = -2$ (bottom fin).

Figure 21.- Concluded.